


Research Article

The Effect of Internalized Paramagnetic Nanoparticles on *Caenorhabditis elegans* Locomotion in the Presence of Magnetic Field

Eleni Gourgou ^{1,2}, Ehsan Mirzakhali, ¹ Yang Zhang,^{3,4} and Bogdan Epureanu¹

¹Mechanical Engineering, University of Michigan, Ann Arbor, MI, USA

²Institute of Gerontology, Medical School, University of Michigan, Ann Arbor, MI, USA

³Electrical Engineering and Computer Science, University of Michigan, Ann Arbor, MI, USA

⁴University of Michigan and Shanghai Jiao Tong University Joint Institute, Shanghai, China

Correspondence should be addressed to Eleni Gourgou; egourgou@umich.edu

Received 23 November 2022; Revised 15 May 2023; Accepted 19 May 2023; Published 10 June 2023

Academic Editor: Hassan Karimi-Maleh

Copyright © 2023 Eleni Gourgou et al. This is an open access article distributed under the Creative Commons Attribution License, which permits unrestricted use, distribution, and reproduction in any medium, provided the original work is properly cited.

Caenorhabditis elegans nematodes are broadly used to investigate the impact of environmental factors on animal physiology and behavior. Here, *C. elegans* with internalized paramagnetic nanoparticles were placed inside a magnetic field (MF) to explore its effects on locomotion. We hypothesized that internalized paramagnetic nanoparticles combined with external MF affect *C. elegans*' locomotion machinery. To test our hypothesis, we used adult *C. elegans* fed on bacteria mixed with paramagnetic nanoparticles of 1 μm , 100, and 40 nm diameter. The presence of nanoparticles inside the worms' body (alimentary canal, body muscle) was verified by fluorescent and electron microscopy. A custom-made software was used to track freely moving *C. elegans* in the absence or presence of MF, sequentially, for 200 + 200 s. We used established metrics to quantify locomotion-related parameters, including posture, motion, and path features. Key attributes of *C. elegans* locomotion (stay ratio, forward over backward motion, speed) were affected only in worms with internalized nanoparticles of 100 nm in the presence of MF (reduced speed, increased stay ratio, decreased forward/backward ratio), in contrast to untreated worms. Our work shows that internalized particles of specific properties affect *C. elegans* locomotion under MF. Hence, it contributes to clarifying the effects of MF and activated nanoparticles on *C. elegans* locomotion, thus fueling further research.

1. Introduction

The effects of magnetic field (MF) on living organisms have been a target of numerous research efforts, with their number increasing significantly during the last decades [1–3]. In addition to the interest the scientific community shows on the impact of alternating MF on cells [4–6], the effects of static MF have also gained attention [7, 8], often with respect to complicated cellular processes like apoptosis [9]. The least studied type of MF, with respect to living cells, is MF of spatial gradient, even though the theoretical framework for the possible impact of high-gradient MF of various sources on cell's molecular components and function is known [10].

Model organisms have been a successful resource to study MF effects on various types of cells and tissues [11–14].

Invertebrate models, like *Drosophila melanogaster*, have been used since the 1980s [15–20]. The nematode *C. elegans*, an emblematic model organism to study the impact of environmental factors on behavior and physiology [21–25], was used in MF-related work only recently [26–30]. Excitingly, the first animal magnetosensory neurons were identified in *C. elegans* [26], which were found to orient to the earth's MF during vertical burrowing migrations, rekindling interest in the field [31–34]. The presence of biogenic magnetite has also been reported in *C. elegans* [35].

Nanoparticles uptake by *C. elegans* worms has been a successful means to evaluate the toxicity of heavy metals and pollutants [36–38], and the importance of *C. elegans* as a model system for *in vivo* nanoparticle assessment has been highlighted [33, 39]. Worms' behavior [40] and locomotion

[33, 41, 42] have been evaluated under the influence of internalized metal nanoparticles, yielding interesting results. In addition, magnetized nanoparticles have been used to activate ion channels in *C. elegans* through heating [43], and internalized nanoparticles were used to locally enhance MF in the worms' body to study the subsequent impact on its metabolism [44].

C. elegans locomotion has been a major behavioral output used to investigate the impact of genetic background, environmental factors, and diverse treatments on the worm's nervous system [45–50]. Locomotion features have been characterized and quantified extensively and are being used as an indicator of *C. elegans* physiological status and health span [51–54]. With respect to *C. elegans*' locomotion in the presence of MF, besides the impact of the earth's MF [26, 55], the literature is sparse. It is reported that nematodes are not affected by mild static MF [27] and that their locomotion can be manipulated by magnetically responsive structures [56], but other than that not much is known about the impact of MF on *C. elegans*' locomotive machinery.

The need to clarify MF effects on animal physiology, and the increasing interest in the sensitivity of *C. elegans* to MF despite the current gaps in the literature, indicate that a detailed investigation of MF gradient effects on worms' behavior can provide important insights. In this context, we hypothesize that internalized paramagnetic nanoparticles combined with external MF affect *C. elegans*' locomotive behavior. To test our hypothesis, we use internalized paramagnetic nanoparticles to generate an effect inside the worms' body, in the closest possible proximity with tissues and cells. We select locomotion as a quantifiable behavioral expression to determine the effect of MF combined with internalized nanoparticles because of its role in animal fitness and as a reliable readout of physiological changes. Our results demonstrate a response of *C. elegans* locomotion machinery to internalized paramagnetic nanoparticles in combination with MF gradients, and they pave the way for future studies seeking to clarify the participation of excitable cells, muscles, and potentially even neurons, to this uncharacterized behavior.

2. Results

2.1. Magnetic Field Gradient Characterization. Simulation results for the two electromagnets used in the study agree with experimental results provided by the manufacturer (Figure S1). A schematic of the MF around the electromagnets and the computational domain of the COMSOL model are presented in Figure 1(a). A view of the MF on the plane of the worm plate surface is presented in Figure 1(b). The direction of the MF between the two electromagnets is indicated by arrows. Contours of MF intensity confirm that the MF is stronger near the electromagnets, as expected.

We focused on the MF and the forces it generates on particles located on the experimental plate surface, where the worms' locomotion takes place. The MF was almost one-dimensional on the plate surface and was strongest near the electromagnets (Figure 1(c)). There were nine

components for the gradient of the MF. In Figure 1(d), the strongest component of the MF gradient is shown (B_{xx}), which is parallel to the x -axis. The magnitude of the gradient was the largest near the electromagnets.

Nanoparticles create secondary MFs and forces in the presence of an external MF. Details regarding the computation of forces created by nanoparticles can be found in the Supplementary Information. The MF flux values for three nanoparticles located along the x -axis and separately the y -axis were calculated in MATLAB using Equations (2) and (3) of Supplementary Information (Figure 2(a)–2(d)). As expected, the MF was strongest close to the particles for both locations and decayed rapidly as the distance from the particles increased (Figure 2(e)). The force between particles located along the x -axis was attractive, while the force between the particles located along the y -axis was repulsive. The attractive forces between the particles allow them to form chain-like structures if they are not interrupted by the medium in which the particles are located [57, 58]. The magnetic moment of the external MF for the particles on the worm plate surface is depicted in Figure 2(f).

2.2. Confirmation of Nanoparticles Uptake and Particle Localization in *C. elegans*' Body. Nanoparticles mixed with bacterial food (*Escherichia coli* OP50) were successfully internalized, as verified by microscopy methods and selected according to the properties of each particle group (Figure 3). The presence of 1 μm paramagnetic particles (Table 1) in the worm's intestine and in the pharynx around the grinder area was verified by bright field microscopy. The particles appear as dark (copper-colored) aggregates accumulated in the alimentary canal (Figure 3(a), right panel), whereas the control animals' intestine area appears transparent (Figure 3(a), left panel). Uptake of 100 nm fluorescent, paramagnetic particles (Table 1) was verified by fluorescent microscopy. The particles appear to accumulate along the intestine lumen and in the pharynx, as shown when filters for rhodamine, the fluorescent substance with which the particles were coated (see Table 1 for particles' properties), were used (Figure 3(b)). Successful feeding on 40 nm paramagnetic particles (Table 1) was confirmed by scanning electron microscopy. When using the circular backscatter detector, 40 nm particles were visualized as white dots under the worm cuticle, in the broad area downstream of the pharynx and along the alimentary canal (Figure 3(c)). The deformation of the sample due to the process followed allowed only for estimating the approximate location of the particles. The white dots which represent the particles appear in different sizes, which might be attributed to particle aggregates or to the different depths at which the particles were located.

To investigate the particles' localization in the worms' body and to explore whether they passed the intestine barrier, we used transmission electron microscopy (TEM). TEM images show that particles can be found in the intestine (40 nm, Figure 4(d)) and the intestine lumen (100 nm, Figure 4(e)). Interestingly, particles' aggregates were also detected inside muscle tissue, very close to the body wall (40 nm, Figure 4(f)). Therefore, the nanoparticles can be in close proximity to excitable cells.

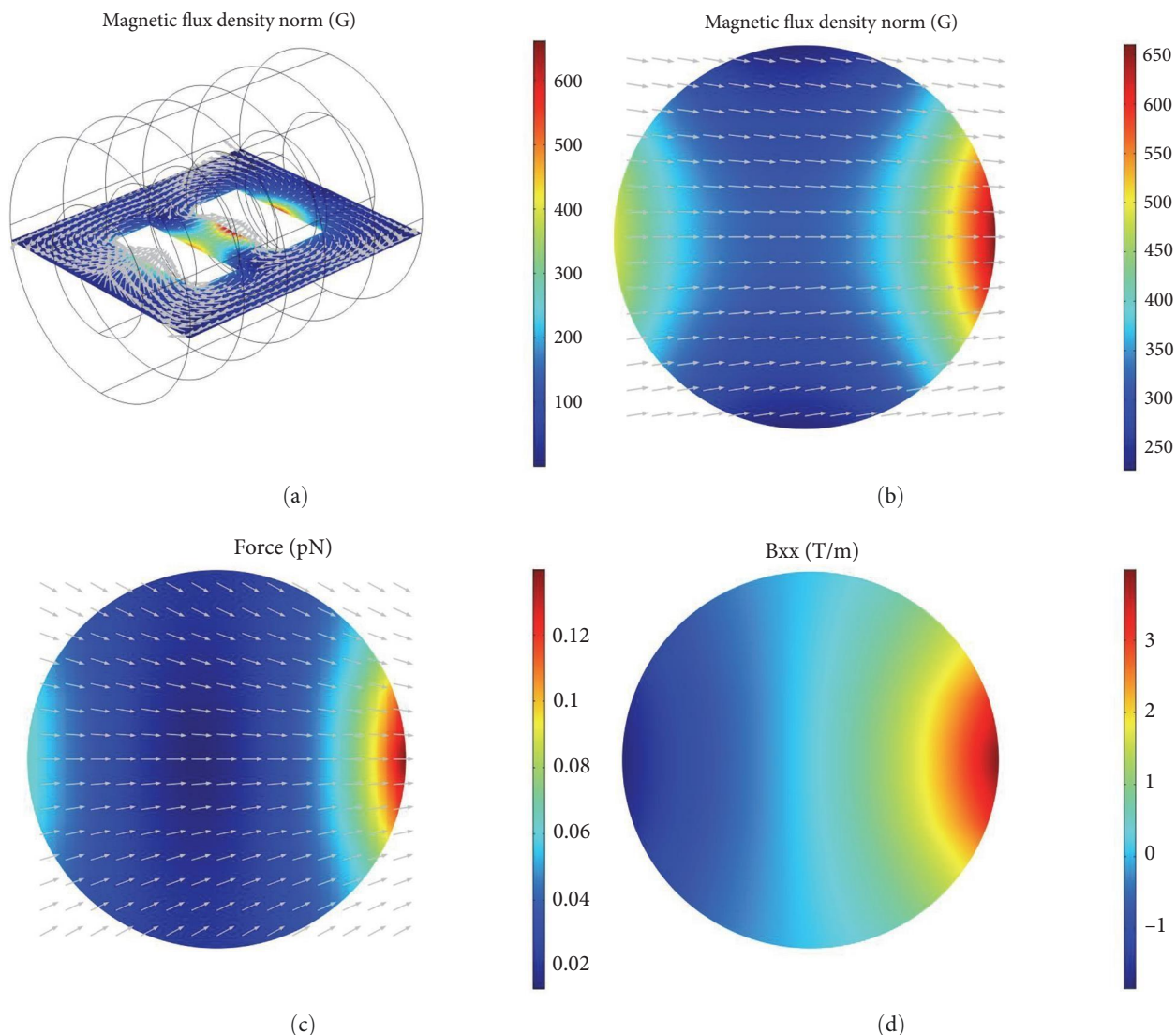


FIGURE 1: COMSOL multiphysics simulation results for the magnetic field (MF) generated by the electromagnets. (a) Overview of the MF flux density on the plane of the worm plate surface. The arrows show the direction of the magnetic flux. (b) The MF flux density distribution on the worm plate surface. The arrows indicate the direction of the MF (the component of the MF in the perpendicular direction is set equal to zero to avoid arrows going in/out of the plane). (c) The magnetic forces are applied on particles located on the plane of the worm plate surface. The arrows show the direction of the magnetic forces (the component of the force in the perpendicular direction is set equal to zero to avoid arrows going in/out of the plane). (d) The gradient of the MF in the direction of the axis that connects the centers of the two electromagnets.

2.3. Analysis of *C. elegans* Locomotion. We examined posture, motion, and path features [59]. The posture feature quantified was the number of bends (bend count), the motion features included are related to motion state (forward/backward ratio and stay ratio) and traveling speed ($speed$, $speed_x$, and $speed_y$), and the path features were the path curvature and the range (see Section 5).

First, we explored whether there are differences in locomotion features due to the presence of nanoparticles alone in the absence of MF. We compared the three groups of particle-fed nematodes to untreated worms when the MF was OFF (Figure S4). No statistically significant difference was detected between untreated and particle-fed animals in the absence of MF (Figure S5).

Next, the particle-fed nematode groups were analyzed during the OFF and ON states of the MF. Results show that only worms fed with 100 nm diameter paramagnetic nanoparticles were affected as they moved freely in MF, compared to nematodes without internalized nanoparticles (Figure 5). More specifically, the number of bends (bend count) realized per worm was not affected in any of the nematode groups (Figure 5, superpanel (a)).

The forward/backward ratio (time the worm was in the forward/backward state over the total recording time) of Group 100 worms decreased when the MF was ON (Figure 5(b1)) and their stay ratio (the time the worm was in the paused state over the total recording time) increased (Figure 5(c1)), indicating an overall decrease of motility. Moreover, the speed of

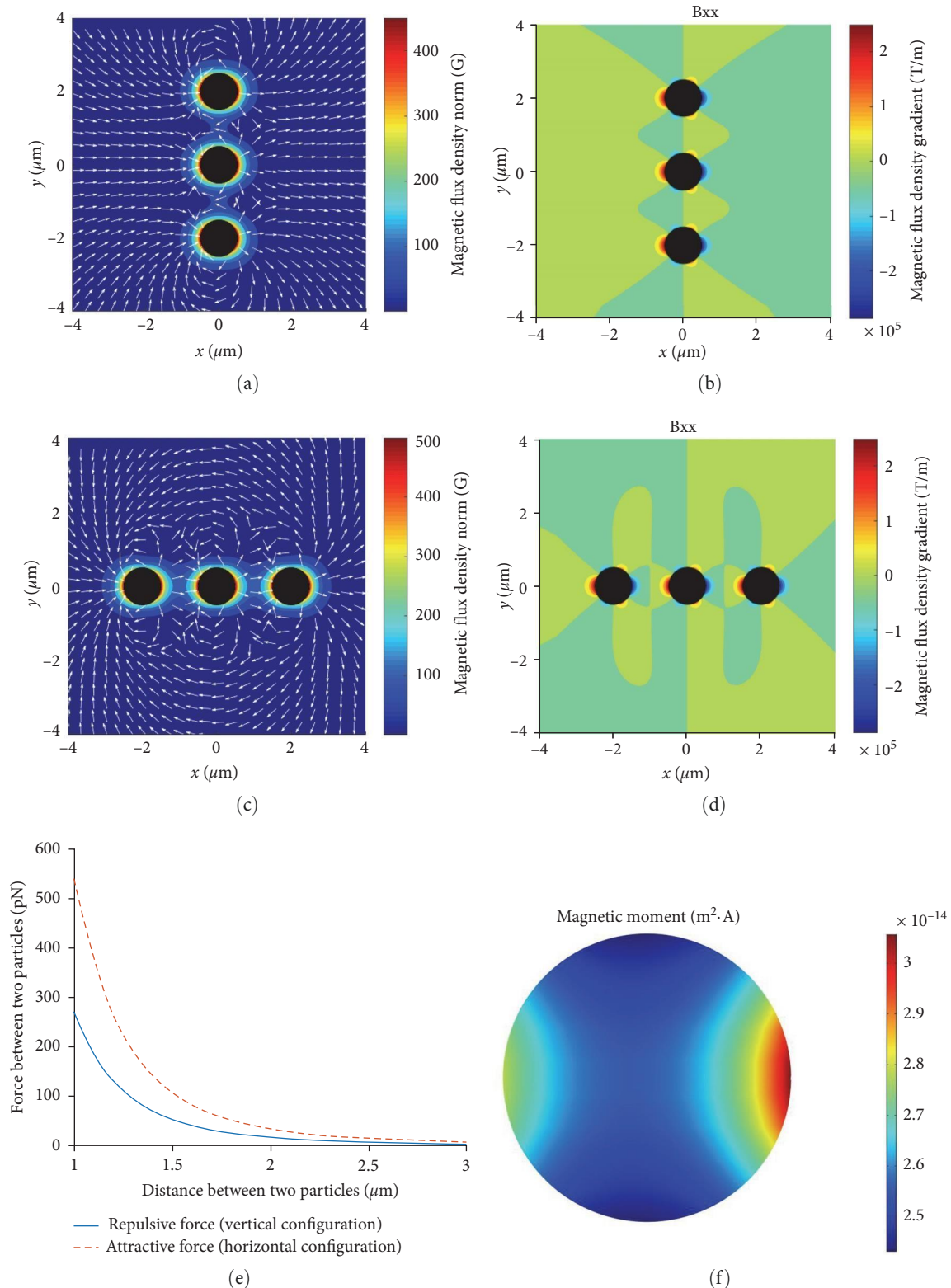


FIGURE 2: Characterization of the magnetic field (MF) around the 1 μm nanoparticles for two different configurations. The direction of magnetic moment for both configurations is along the x -axis, as is shown in Figure 6. The magnetic moment of the particles is assumed to be similar and equal to the maximum value that is computed from the COMSOL Multiphysics simulations in the plate. (a) The MF flux density around three paramagnetic particles in the vertical configuration, i.e., along the y -axis. The arrows indicate the direction of the MF. (b) The largest component of the gradient of the MF for the vertical configuration of the paramagnetic particles. (c) The MF flux density norm around three paramagnetic particles in the horizontal configuration, i.e., along the x -axis. The arrows indicate the direction of the MF. (d) The largest component of the gradient of the MF for the horizontal configuration of the paramagnetic particles. (e) The forces between two particles in each configuration. (f) The magnetic moment of the external MF, which the particles experience once inside the MF.

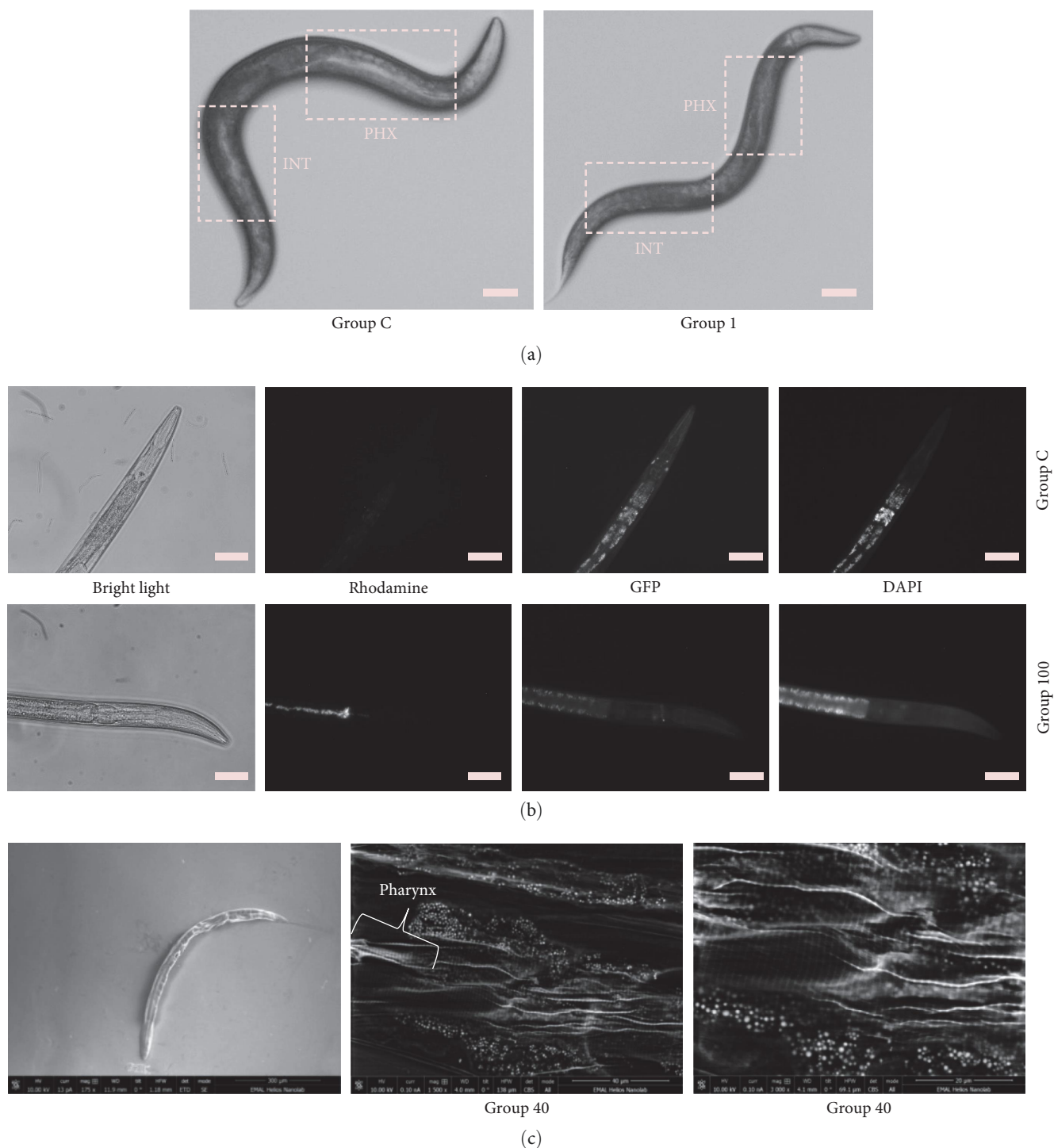


FIGURE 3: Confirmation of nanoparticles uptake in young adult *C. elegans*. (a) Internalization of $1\ \mu\text{m}$ paramagnetic particles is verified by bright field microscopy. Left: worm fed with plain *E. coli* OP50 (control, Group C). Right: worm fed with *E. coli* OP50 mixed with $1\ \mu\text{m}$ particles. Particles appear to be aggregated in the dark-colored pharynx (PHX) and intestine (INT) of Group 1 worms, in contrast to the light-colored PHX and INT of Group C worms. Scale bar: 0.1 mm. (b) Internalization of 100 nm magnetic, fluorescent nanoparticles is verified by epifluorescent microscopy. Top panels: worm fed with plain *E. coli* OP50 (control, Group C), bottom panels: worm fed with *E. coli* OP50 mixed with 100 nm particles. Bright light: worms illuminated by bright light source; rhodamine: worms visualized with optical filter for rhodamine, Excitation 545 nm/Emission 565 nm; GFP: worms visualized with optical filter for green fluorescent protein (GFP), Excitation 395 nm/Emission 510 nm; DAPI: worms visualized with optical filter for DAPI, Excitation 358 nm/Emission 460 nm. In GFP and DAPI images, autofluorescence is the only fluorescence detected. Scale bar: 0.1 mm. (c) Internalization of 40 nm paramagnetic particles is verified by scanning electron microscopy (SEM). Left: a whole *C. elegans* as captured by SEM, using Everhart–Thornley SE detector. Center: 40 nm particles, shown as white dots, detected close to *C. elegans* PHX, using circular backscatter (CBS) detector, magnification 1,500 \times . Right: 40 nm particles, shown as white dots, detected close to *C. elegans* PHX, using CBS detector, magnification 3,000 \times . Location of particles is approximate due to distortion generated during sample processing.

TABLE 1: Groups of worms tested and properties of the respective nanoparticles.

Group	Particle size	Coating	Magnetic properties	Fluorescence
Group C	–	–	–	–
Group 1	1 μm	Streptavidin	Paramagnetic	No
Group 100	100 nm	No	Paramagnetic	Rhodamine
Group 40	40 nm	–COOH	Paramagnetic	No

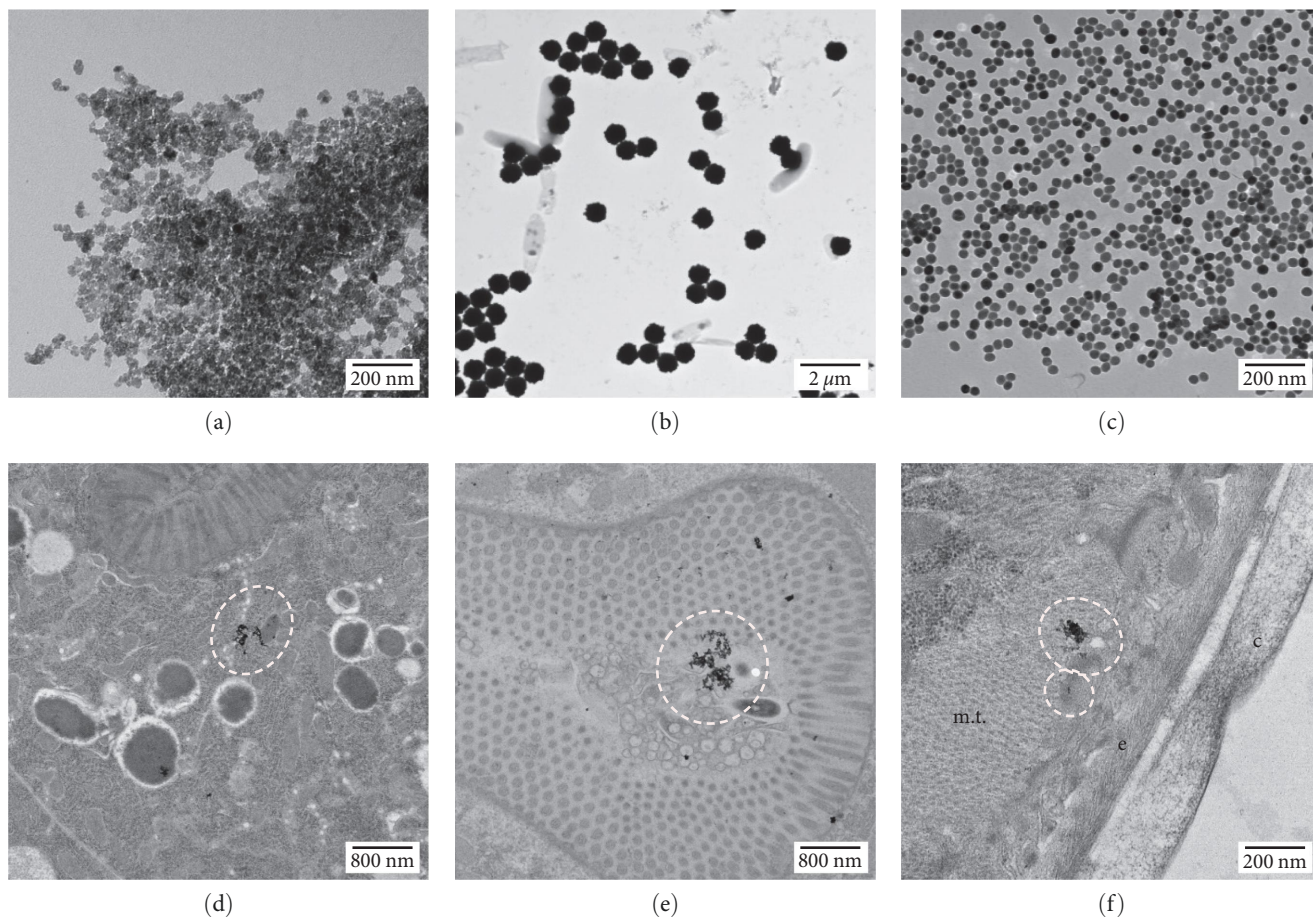


FIGURE 4: Location of nanoparticles in young adult *C. elegans*, using transmission electron microscopy (TEM). (a–c) Free particles (a: 100 nm, b: 1 μm , c: 40 nm) imaged with TEM; (d) 40 nm particles aggregates in the intestine; (e) 100 nm particles aggregates in the intestine lumen; (f) 40 nm particles aggregate in body muscle tissue (m.t.), close to epidermis (e) and cuticle (c). Dotted circles indicate particles' aggregates in all panels.

worms fed with 100 nm particles decreased when the MF was ON (Figure 5(d1)). There was no significant effect detected in the components of the $speed_x$ and $speed_y$ components (Figure 5, superpanels (e) and (f)). A trend for decreased $speed_x$ is apparent, but not statistically significant, in all experiments of Group 100 (Figure 5(e1)).

None of the path features, namely path curvature and range, was found to be affected in a significant and consistent way in any of the groups tested (Figure 5, superpanels (f)–(h)).

3. Discussion

3.1. Internalized Nanoparticles Alone Do Not Affect *C. elegans* Locomotion. *C. elegans* nematodes are shown to be an excellent model for evaluating the impact of nanomaterials on

animal physiology and behavior [60]. More specifically, metal nanoparticles of various types have been used to evaluate particle toxicity using *C. elegans* [42, 61–65]. Particle coating and size, worm developmental stage, and duration of exposure have been shown to affect translocation of particles in various tissues of the worm's body [42, 61, 66]. Particles used in the present study are larger [42, 61–63], and worms have been exposed to them for a shorter period (18–20 hr) than elsewhere [42, 67]. These differences may explain why most of the nanoparticles are found along the worms' pharynx, upper intestine (Figure 3(a) and 3(b)), and lower intestine area (Figure 3(b)). The location of 40 nm particles in worms of Group 40 around the pharynx and grinder area (Figure 3(c)) is only approximate, as some deformation has been induced on the sample during

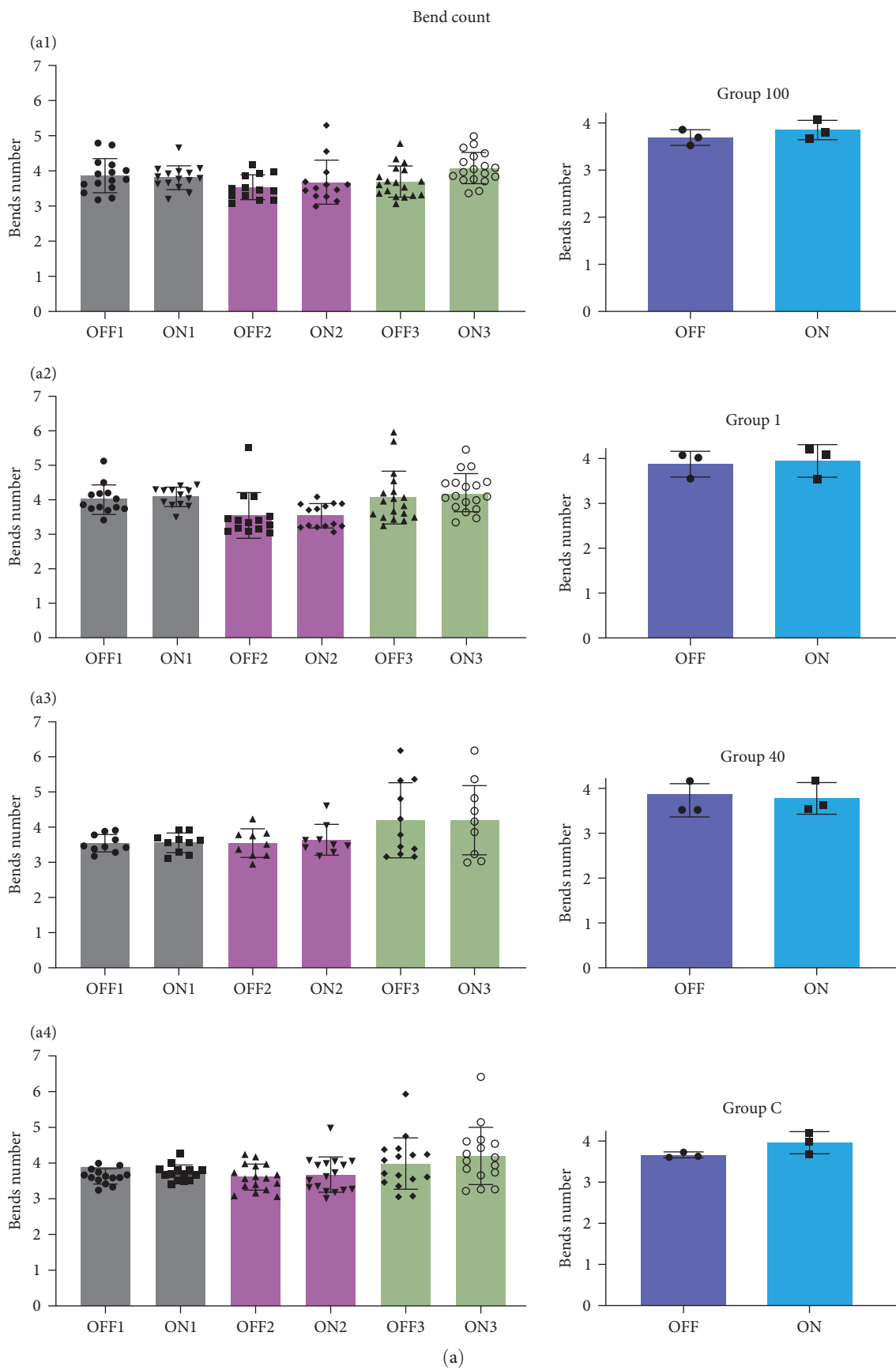


FIGURE 5: Continued.

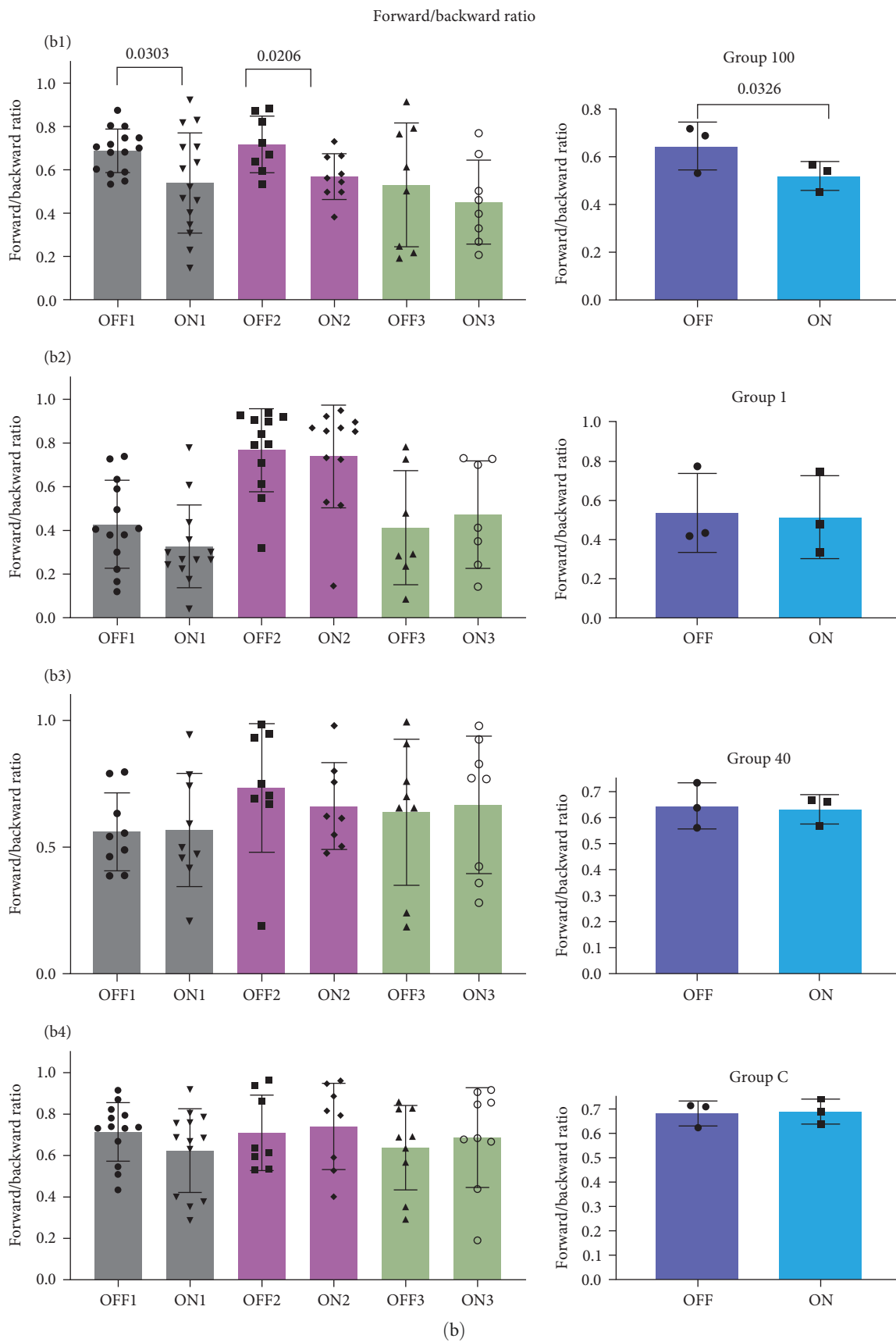


FIGURE 5: Continued.

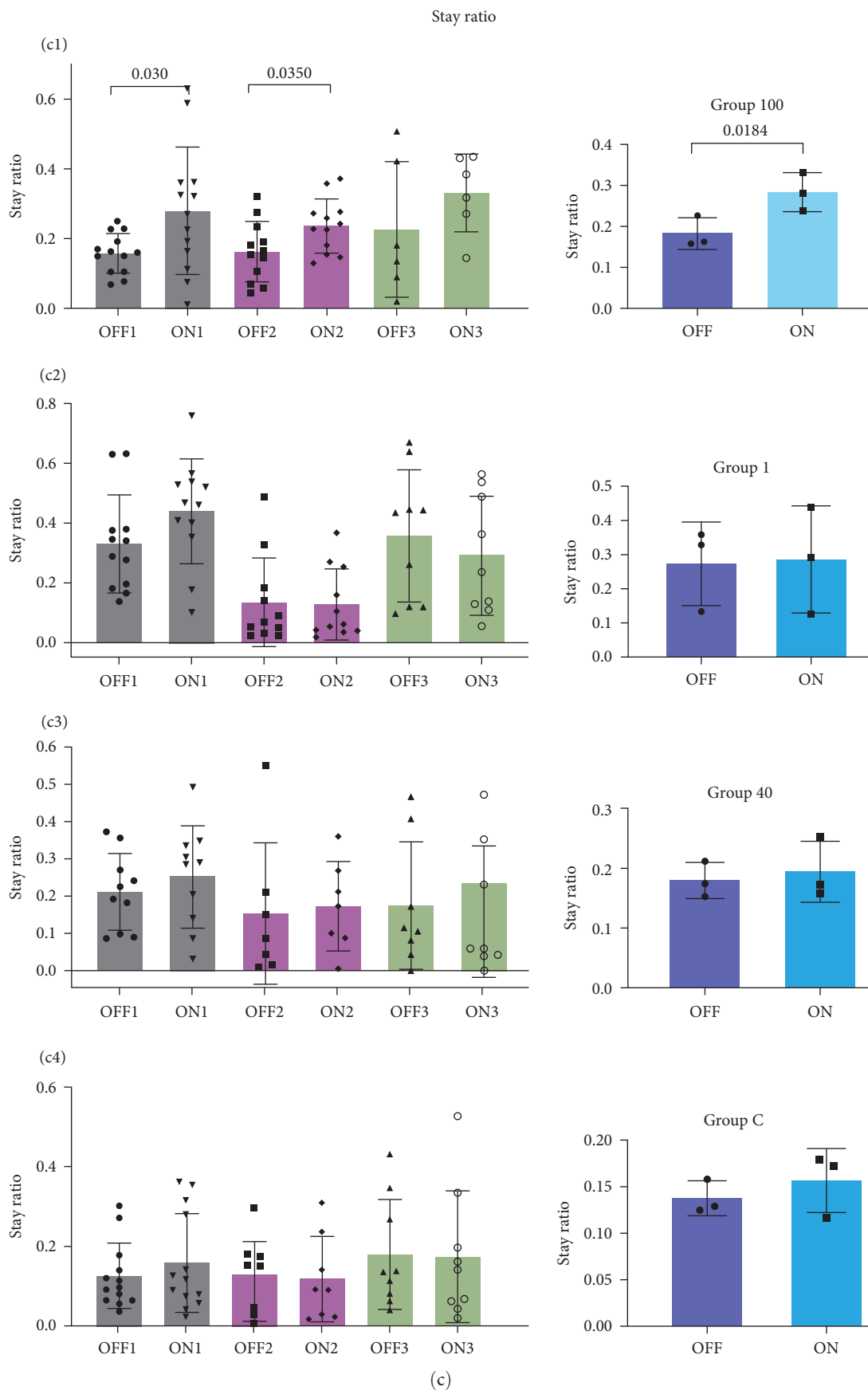


FIGURE 5: Continued.

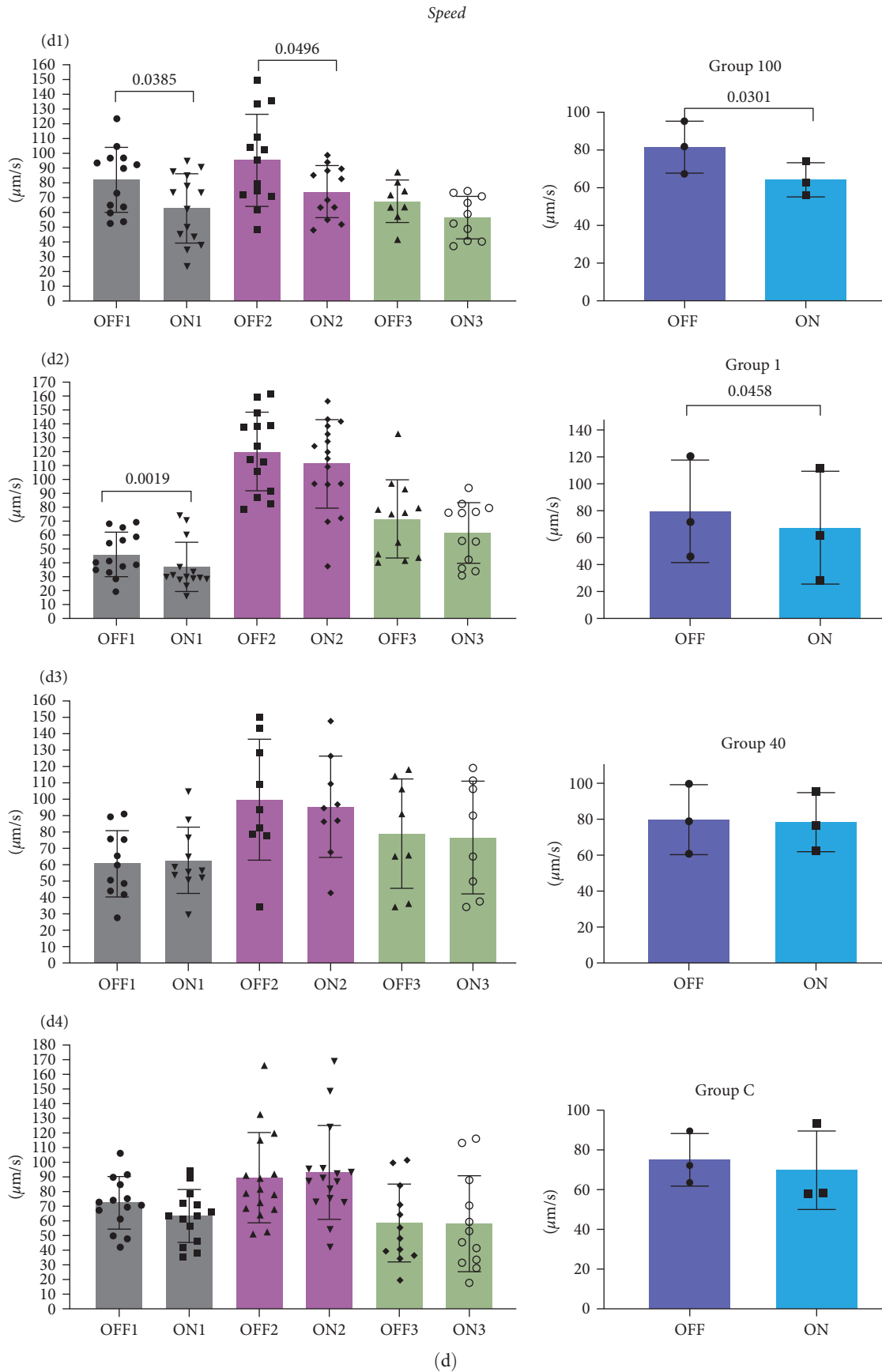


FIGURE 5: Continued.

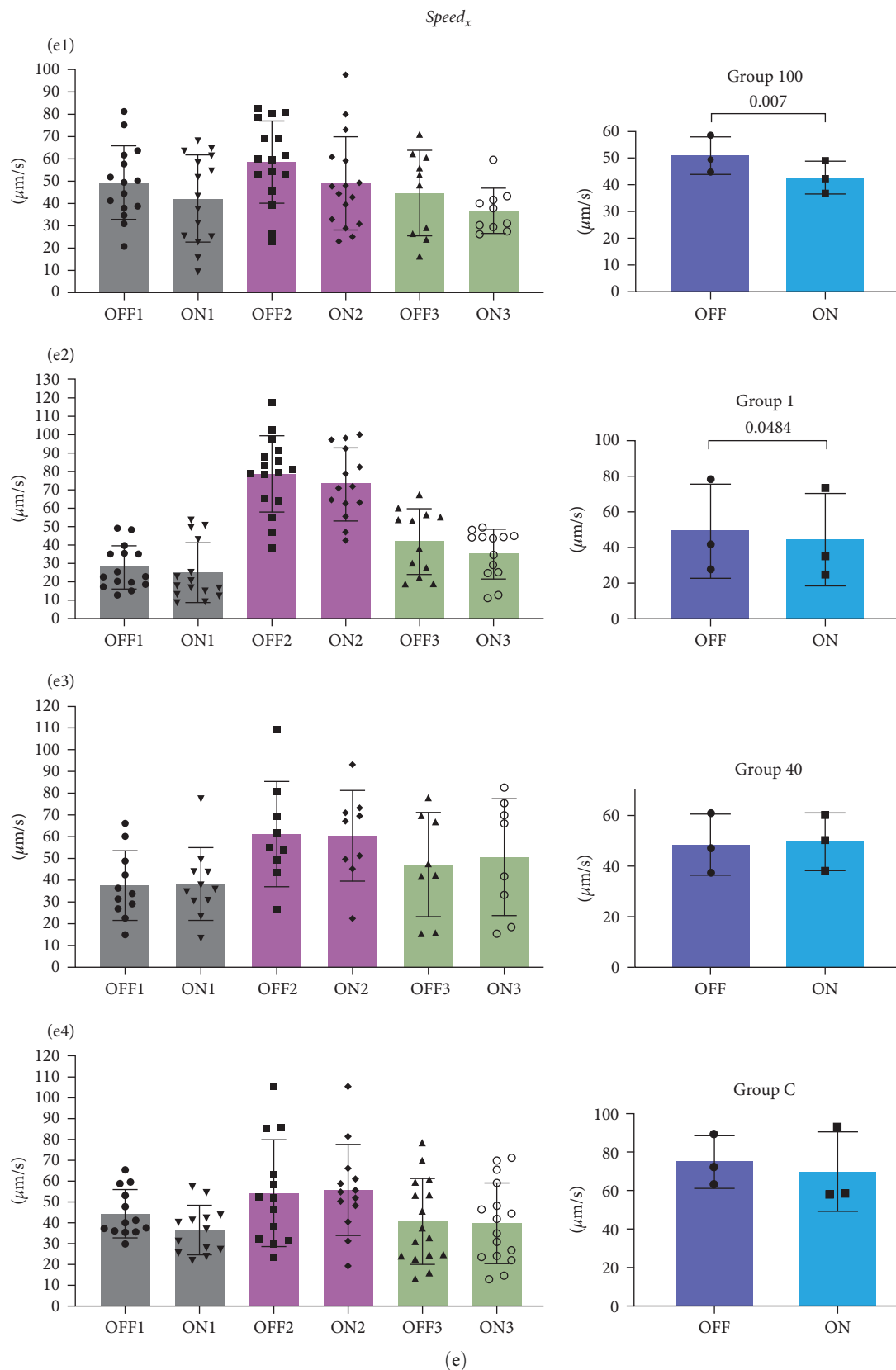


FIGURE 5: Continued.

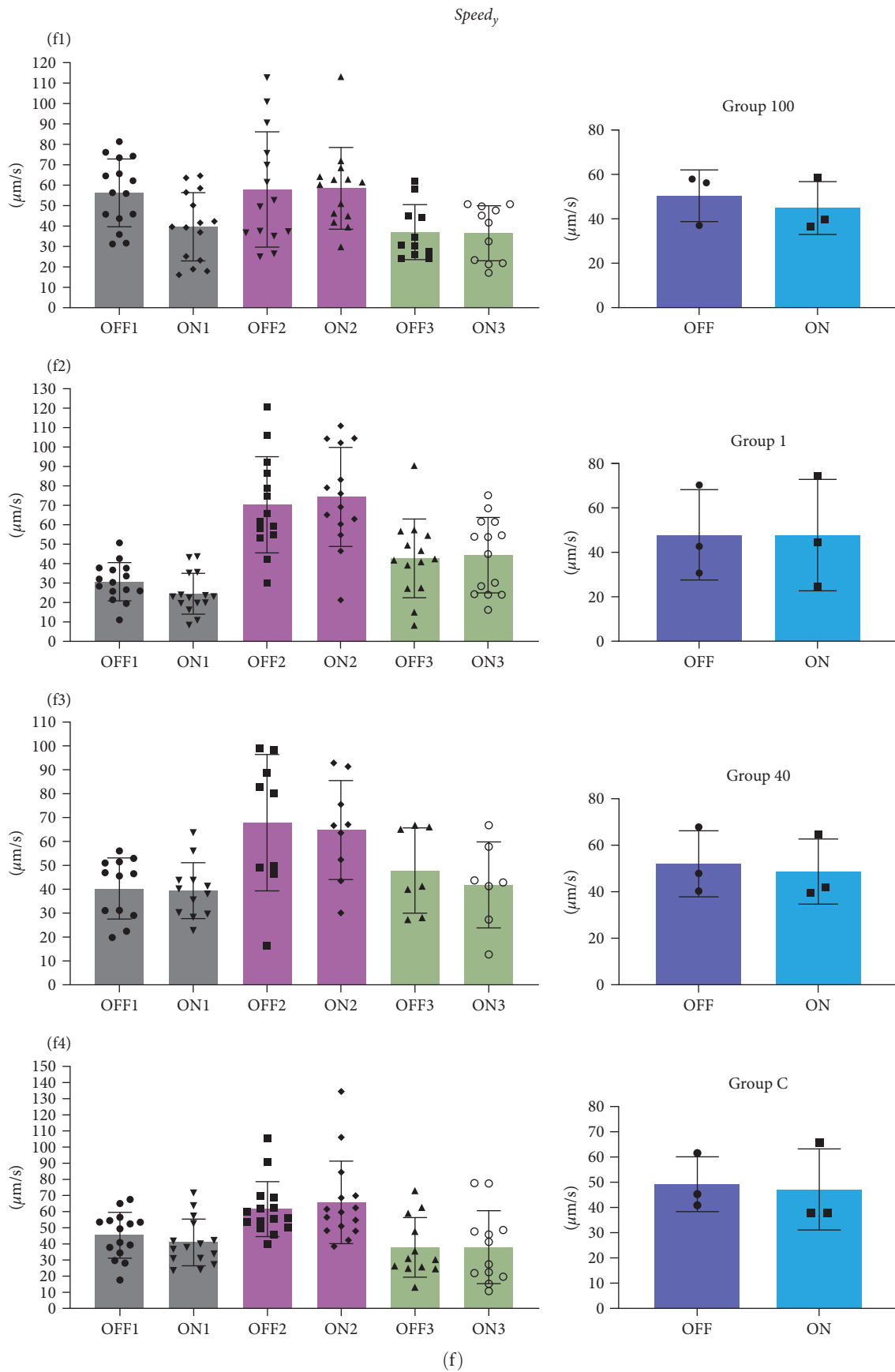


FIGURE 5: Continued.

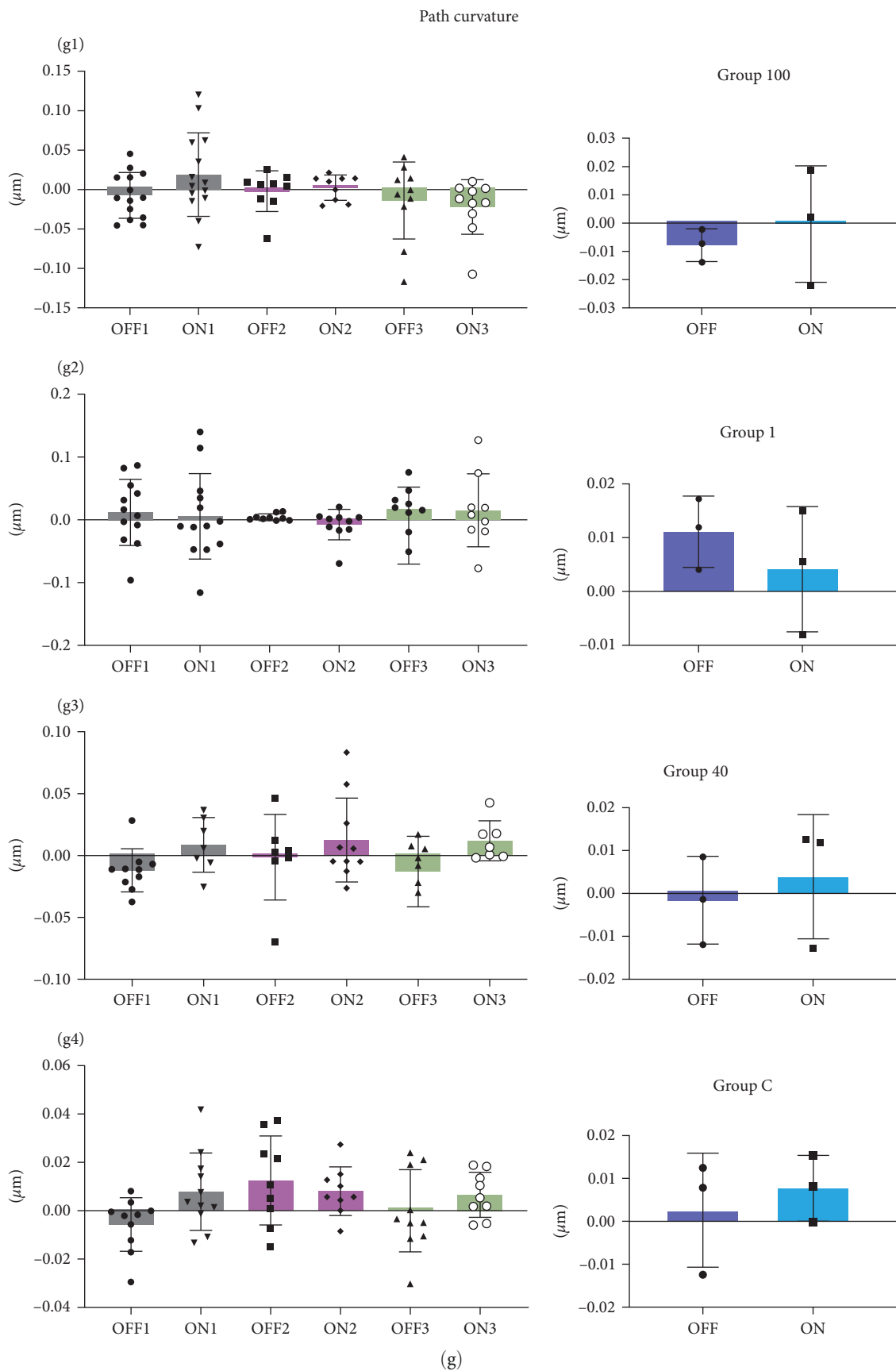


FIGURE 5: Continued.

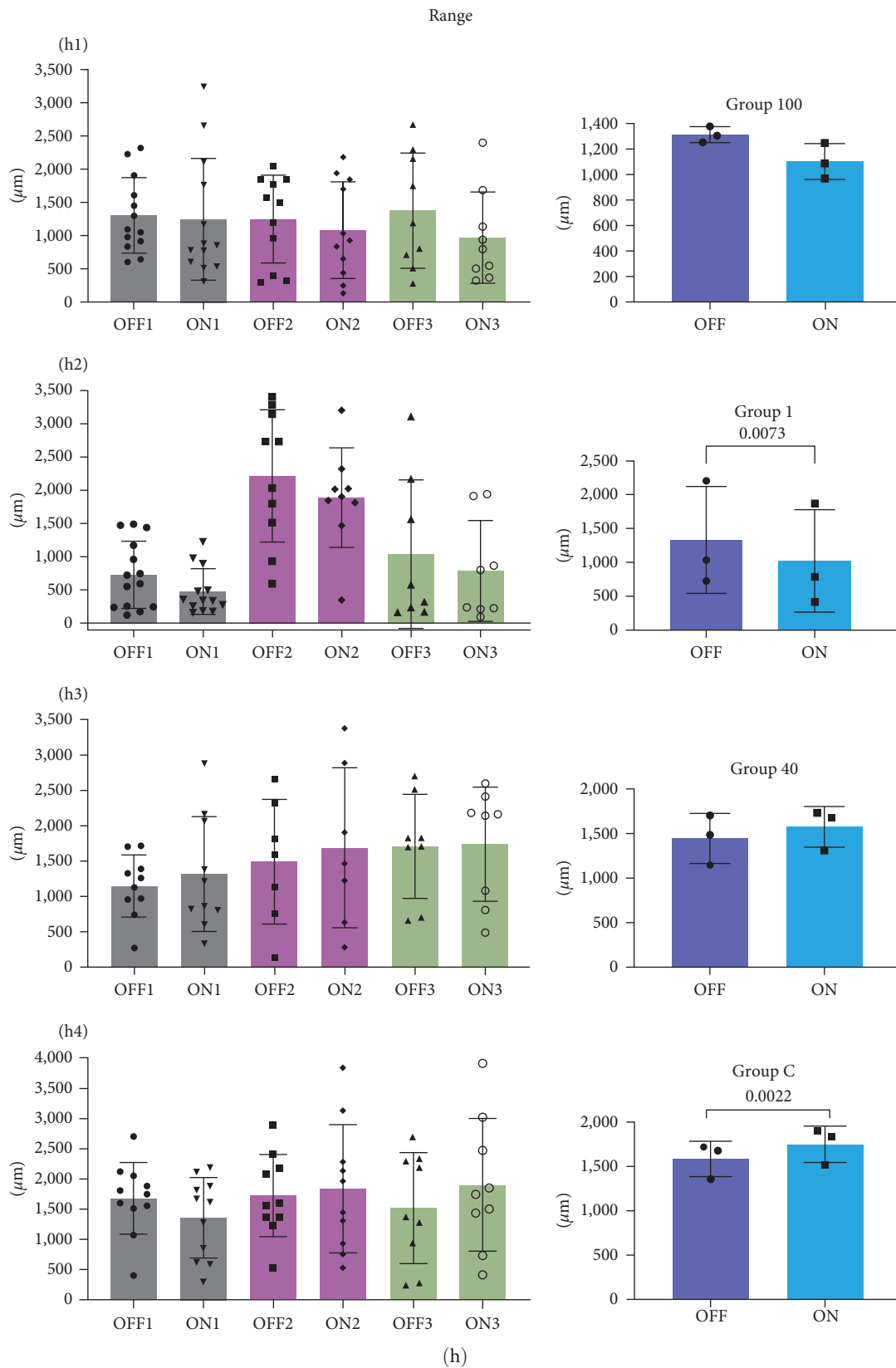


FIGURE 5: Locomotion features and their metrics, as they have been quantified for all four groups of worms tested in the absence (OFF state) or in the presence (ON state) of external magnetic field (MF). For each group, tested worms were tracked in three independent experiments conducted on three experimental days (OFF1/ON1, OFF2/ON2, OFF3/ON3). (a–h) (all) superpanels eight locomotion features have been quantified: (a) bend count, (b) $speed_x$, (c) $speed_y$, (d) $speed_z$, (e) forward/backward motion ratio, (f) stay ratio, (g) path curvature, and (h) range. Group 100 (grey plots): fed on *E. coli* OP50 mixed with 100 nm-diameter iron core paramagnetic particles, $n = 33$ ($n_1 = 13$, $n_2 = 11$, $n_3 = 9$); Group 1 (pink plots): fed on *E. coli* OP50 mixed with 1 μm -diameter paramagnetic particles, $n = 32$ ($n_1 = 14$, $n_2 = 10$, $n_3 = 8$); Group 40 (lime plots): fed on *E. coli* OP50 mixed with 40 nm-diameter iron core paramagnetic particles, $n = 25$ ($n_1 = 10$, $n_2 = 7$, $n_3 = 8$); Group C:

control animals, fed on plain food source *E. coli* OP50, $n = 30$ ($n_1 = 11$, $n_2 = 10$, $n_3 = 9$). Graphs compare ON and OFF results from each experiment (a–h, left panels) and from all three experiments combined (a–h, right panels). Subpanels of rows a1–h1 display results for Group 100, rows a2–h2 results for Group 1, rows a3–h3 results for Group 40, and rows a4–h4 for Group C. Comparisons were made by applying Student's *t*-test (unpaired for individual experiments, paired for combined data); any difference was considered statistically significant when $p \leq 0.05$, only statistically significant differences are shown. We consider a locomotion feature to be affected by internalized paramagnetic particles in the presence of MF only when there is a statistically significant difference detected on at least two experiments and when comparing combined data. Therefore, only speed (panel b1), forward/backward motion ratio (panel e1) and stay ratio (panel f1) for Group 4 nematodes are significantly affected.

preparation, and scanning electron microscopy (SEM) allows for detecting objects that are close to the body surface. Particles' aggregates are also found in the intestine (Figure 4(d)), intestine lumen (Figure 4(e)), and in muscle tissue (Figure 4(f)).

Worms used in the present work are young adults and not larvae [42, 66, 67], which, as developing organisms, could be more vulnerable to toxic effects [68]. Moreover, particles used in the experiments presented here are larger [42, 61–63] and made of different metals [41, 63], compared to the ones utilized in similar studies, which may result in different abilities to overcome the intestine barrier or translocate to other tissues, as well as to different toxicity *per se*.

3.2. Internalized Nanoparticles, Combined with MF, Have a Particle-Specific Effect on *C. elegans* Locomotion. Magnetotaxis in *C. elegans* has been demonstrated [26], with the participation of AFD neurons, the first to be identified as magnetosensory in the animal kingdom. It was suggested that endogenous magnetic material, previously reported in *C. elegans*, may be also involved [26, 35]. These findings sparked a vivid discussion in the *C. elegans* community [31, 69–71]. In our experiments, the locomotive behavior of Group C worms, which did not contain any particles, was not affected by the externally applied MF (Figure 5).

At the same time, the presence of 100 nm-diameter internalized nanoparticles had an impact on specific locomotion features (Figure 5) when an MF was applied. Indeed, Group 100 worms move more slowly (Figure 5(b1)), spend less time moving, either forward or backward (Figure 5(e1)), and spend more time in the paused state (Figure 5(f1)). Therefore, the overall motility of these nematodes is decreased [33]. Modulation of the locomotive circuitry, including the switch from a more mobile to a less mobile state, is known to be mediated by dopaminergic neurons [72, 73], like the PDE mechanosensory neuron. Our findings set the stage for investigating one more role for dopamine as a potential regulator of behavioral plasticity in 100 nm-diameter particle-fed *C. elegans* inside MF.

It is possible that worms slowed down when they found themselves in a particular orientation inside the MF or when the internalized particles obtained a particular orientation with respect to the MF. As indicated in Figure 1, the properties of the MF change significantly in the direction of the MF. Therefore, any effect the MF may have on the particle-fed worms or on the internalized particles themselves could be changing when worms are moving along the MF.

There was no effect detected in Group 40 in any of the metrics examined. This can be due to the smaller MF or smaller gradient of MF of the particles in this group. Therefore, even though they are found in the intestine and close to

the body wall muscles (Figures 4(d) and 4(f)), they are not potent enough to generate any detectable effect. Similarly, there was no impact detected in Group 1 nematodes. This suggests that it may be difficult for particles of this size to cross tissue barriers in the worms' body and end up close to excitable cells. Indeed, although aggregates of 1 μm particles were spotted in the alimentary canal (Figure 3(a)), they were not detected at other locations by electron microscopy.

In parallel, we have been able to estimate the MF and the gradient of MF only for the 1 μm particles due to lack of available information on the magnetic properties of the 40 and 100 nm particles. Nonetheless, we can compare the MF and gradient of MF between the particles based on their size (see Supplementary Information). We found that smaller particles have a larger gradient of MF compared to larger particles in their proximity. The overall impact each particle type has on worms' physiology depends on the magnitude and the gradient of the MF. Both depend on the material properties of the particles, which determine the magnetic moment. Our experimental observations show that the strongest effect among the three types of studied particles occurred in the case of 100 nm particles.

The particles' coating (Table 1) was not expected to affect their magnetic behavior. It could, however, impact their interaction with cells. Since the magnetic and physical properties of the particles are the most influential regarding the secondary MF effects, we focused on the particle size for our data analysis. In addition, the thickness of the coating was small (a single monolayer of streptavidin for the 1 μm particles and a 2–3 nm thick layer of polymer for the 40 nm particles, according to the manufacturers), which means that the magnetic core could still affect cells and tissues close to the particle. The experimental procedure did not allow us to know the quantity of particles ingested by each individual worm, nor the exact location and the precise interactions of particle aggregates in each individual nematode. Therefore, we cannot draw conclusions based on the particles' quantity or exact aggregate location inside each worm tested.

Ideally, results shown in Figures 1 and 2 should be combined to assess the synergistic properties of the external component of the MF (generated by the electromagnets) and of the secondary component of the MF (generated by the magnetized particles). However, the MF generated by the particles is very localized (in the microscale), as shown in Figure 2. Thus, we discuss below the potential effects of the MF induced by the electromagnets and of the secondary MFs separately and on their own respective scale. We also discuss the effect of particles' aggregates behavior under the influence of an external MF.

3.3. Factors that Could Shape the Impact of Internalized Particles in the Presence of External MF. The forces that were created either by the external MF or the paramagnetic particles themselves were small (Figure 2(e)), and they were not strong enough to mechanically push the worms to move along their track. This suggests that some other mechanism is responsible for the detected changes in worms' locomotion. The magnitude of the external and secondary MFs had the same order of magnitude, and they were small (Figures 1 and 2(a) and 2(c)). However, the gradient of the MF fields in the vicinity of the particles was substantially large (Figures 1(b) and 1(d)).

Effects were likely to be more pronounced where the external MF was stronger since that would result in stronger secondary MFs generated by the particles (until the magnetization of the particles becomes saturated). Therefore, the locomotion of worms crawling under stronger MF, namely near the electromagnets (Figure 1), was more likely to be affected. The spatial distribution of the MF can partly explain the variations observed in the experiments. In addition, the presence of a worm crawling into areas of higher magnetic flux, therefore of higher impact, is a random event. The variations in the values of the metrics examined might mirror that randomness. Lastly, since we had no direct control over the location where particles resided in the worms' body, their presence in body locations where they could affect mechanosensitive ion channels could be another explanation for the variability that we observe in our experiments (indicative cases: Figure 5(b1), ON1; Figure 5(c1), ON1; Figure 5(c2), ON1; Figure 5(c3), ON1).

Zablotskii et al. [10] provide several examples in which the gradient of MF can affect cellular and subcellular mechanisms. The gradient of the secondary MF fields obtained from our simulations (up to 2×10^5 T/m for the $1 \mu\text{m}$ particles, Figures 2 (b) and 2(d)) was well above the threshold that Zablotskii et al. [10] suggest may impact cells with mechanosensitive ion channels (10^3 T/m, see also [10]). The gradient of the secondary internal MF fields was also above the threshold the same authors pose for magnetically induced changes in gene expression; however, we consider such a possibility highly unlikely in our case due to the very short time the external MF was applied (~ 90 s). Therefore, the secondary field generated by the paramagnetic particles upon application of external MF could lead to local gradients of MF inside the worm's body, large enough to interfere with the functionality of excitable cells (e.g., body muscle cells, see also Figure 4(f)).

This could have happened by affecting the cells' ion channels, provided that the particles were very close or even in contact with the cells' membrane. Experimental data presented here cannot provide insight into exactly which cells might have been the target of the observed MF effect. However, TEM findings (Figure 4) showed that particles' aggregates could be located in body wall muscles (Figure 4(f)). Therefore, the possibility that excitable, e.g., muscle cells, were affected by ingested particles in the presence of MF is considerable. In addition, it is possible that mechanosensitive neurons are excited as well, given the conceivable effect of MF on mechanosensitive ion channels, as described earlier [10]. These could be dopaminergic neurons, like PDE, ADE, or CEP [73, 74], or mechanosensitive neurons that innervate the body wall

muscles, like PVD [75]. Moreover, the impact on the intestine (Figures 4(d) and 4(e)) could affect *C. elegans* physiology and locomotion dynamics, given the multiple roles of this complex tissue [76, 77]. Further experiments are needed to clarify the mechanism behind the observed changes.

The possibility of MF having a direct action on the magnetosensitive neurons described in *C. elegans* [26] cannot be excluded. The neurons reported to have a magnetosensory function are the AFD sensory neuron pair [26], which are also known to respond to temperature [78], CO_2 [79], and moisture [80] gradients. Interestingly, AFD neurons can transmit both stimulatory and inhibitory signals to the interneuron AIY, operating as a behavioral regulator in a thermosensory circuit [81]. Whether AFD contributes in a similar way to the behavioral dynamics reported here could be explored in future experiments via calcium imaging of freely moving nematodes under the reported experimental conditions. In the present study, we did not have direct evidence of sensory or motor neurons being affected by MF, neither was that possibility explored.

When an MF is applied to a population of paramagnetic particles, the particles self-organize into arrays, columns, or chains, depending on the nature of the applied MF and the properties of the particle-containing medium [57, 82–84]. In our experiments, when the MF is turned ON, it is likely that the internalized particles start moving as they organize into self-assembled structures. It is possible that this motion applies pressure on or stretches the surrounding tissue, resulting in a decrease in overall motility.

4. Conclusions

We demonstrate a particle-specific effect of internalized paramagnetic nanoparticles, in combination with externally applied MF, on the dynamics of *C. elegans*' locomotion. Established locomotion metrics, i.e., speed and motion state, are significantly different between untreated worms and worms treated with $100 \mu\text{m}$ particles when moving inside an MF. In parallel, no significant difference is detected between untreated and particle-treated worms in the absence of an MF. Possible explanations on the mechanism that leads to the observed results are related to the effects of MF gradients on cells [10, 85] mediated by magnetic nanoparticles [86]. These are also related to the formation of paramagnetic particles' aggregates inside MF [82–84]. The exact mechanism that underlies the observed effect is not clear. Our experiments are the first to comparatively explore the effect of four different types of paramagnetic particles in young adults of an established nematode model system. Our findings pave the way for more targeted experiments on the sensitivity of animals to MF gradients. *C. elegans* nematodes, due to their excellent trackability, could play a key role in such an effort.

5. Materials and Methods

5.1. Magnetic Field Characterization. COMSOL Multiphysics (COMSOL, Burlington, MA) software was used to characterize the MF that is generated by the two electromagnets in the

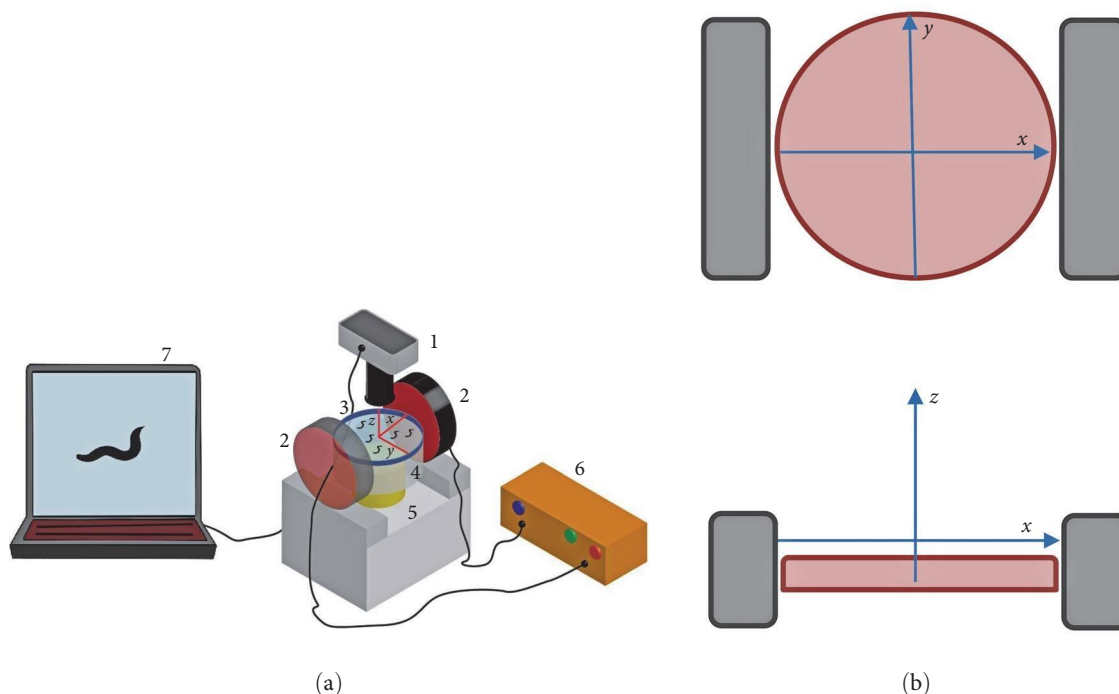


FIGURE 6: Experimental setup: (a) parts of the experimental setup for the application of gradient magnetic field on freely moving *C. elegans*. 1: objective lens and camera; 2: electromagnets; 3: NGM plate with freely moving wild type N2 *C. elegans*, with schematic of plate orientation, red lines indicating x , y , and z axes; 4: auxiliary transparent base; 5: working stage with bright light source; 6: power supply; 7: computer and recording software. Objects are not depicted in scale; (b) schematic of the orientation of the NGM plate (pink circle), x , y , and z axes and electromagnets (gray rectangles), top: view from above, bottom: view from aside.

experimental setup (Figure S2). The data for the magnetic flux density of the electromagnets (available from the manufacturer) was used to calibrate the parameters of the electromagnets in COMSOL Multiphysics. The COMSOL Multiphysics model was also used to estimate the intensity of the external MF, the gradient of the external MF, and the forces that are applied on paramagnetic particles by the external MF. MATLAB was used to calculate the forces applied on the paramagnetic nanoparticles. More details are given in the Supplementary Information section.

5.2. Nanoparticles Internalization. We investigated the locomotion of four groups of young adult wild-type N2 *C. elegans* hermaphrodites fed on (see also Table 1):

- (i) plain bacterial food source *E. coli* OP50, control animals-Group C, $n = 30$,
- (ii) *E. coli* OP50 mixed with $1\ \mu\text{m}$ -diameter paramagnetic particles (Dynabeads MyOne Streptavidin C1, Invitrogen, Thermo Fisher Scientific, USA), Group 1, $n = 32$,
- (iii) *E. coli* OP50 mixed with $100\ \text{nm}$ -diameter paramagnetic particles (nanomag-CLD-red, Micromod Partikeltechnologie GmbH, Germany), Group 100, $n = 33$, and
- (iv) *E. coli* OP50 mixed with $40\ \text{nm}$ -diameter paramagnetic particles (iron oxide nanocrystals, Ocean Nano-Tech, USA), Group 40, $n = 25$.

In all cases, particles were isolated from the initial suspension by brief centrifugation and were resuspended in OP50 in a final concentration of $0.5\ \text{mg/ml}$ OP50-particle mix. Freshly made $60\ \text{mm}$ standard nematode growth medium (NGM) plates were seeded with $100\ \mu\text{l}$ of plain OP50 or OP50-particle mix. Plates were left to dry overnight at room temperature (RT), and ~ 20 worms were transferred in them the next day. Nematodes were left to feed on the plain or enriched bacterial lawn for $18\text{--}20\ \text{hr}$ at 20°C . Then, they were either prepared for microscopy or $12\text{--}15$ of them were transferred to a fresh, unseeded $35\ \text{mm}$ NGM plate for locomotion recording. In the second case, worms were left to acclimatize in the new plate for $\sim 15\ \text{min}$ before recording. There were three reasons for transferring worms to a new, smaller plate. First, we wanted the worms to experience the effect of only internalized nanoparticles under MF and not of the remaining particles on the plate surface. Second, the presence of enriched bacterial lawn on the plate surface interfered with the tracking algorithm and could have affected the worms' locomotion due to its viscosity. Third, by using $35\ \text{mm}$ plates, we decreased the distance between the electromagnets and the worms (as shown in Figure 6) so that the worms experience a stronger external MF.

For each group tested, experiments were run over three different experimental days. Therefore, on each experimental day, we processed $10\text{--}14$ worms for a specific group. These $10\text{--}14$ worms were treated simultaneously (on the same

plate), and each one of them is considered a biological replicate.

5.3. Fluorescent, Scanning, and Transmission Electron Microscopy (SEM and TEM)

5.3.1. Fluorescent Microscopy. Worms were transferred to an unseeded NGM plate and were washed with 0.5 ml of 1× phosphate-buffered saline (PBS). Next, they were transferred to a glass slide, where they were anesthetized on fresh agar pads [87] using 10 mM NaN₃ [88]. Samples were imaged using a BX51WI Olympus fluorescent microscope (Olympus, Tokyo, Japan) coupled with an ORCA-flash4.0 camera (Hamamatsu Photonics, Hamamatsu City, Japan).

5.3.2. Scanning Electron Microscopy. Samples were prepared as described previously [87, 89], with modifications and dissection omitted. Briefly, worms were transferred to an unseeded NGM plate and were washed with 0.5 ml of 1× PBS. Next, they were transferred to a glass coverslip and were anesthetized using 10 mM NaN₃ [88]. Samples were imaged using FEI Helios 650 nanolab SEM/FIB (FEI, Thermo Fisher Scientific, Waltham, MA).

5.3.3. Transmission Electron Microscopy. Samples were prepared based on the literature [90, 91], with modifications. Briefly, tissues were fixed in pre-warmed 3.2% paraformaldehyde, 0.2% glutaraldehyde in 0.1 M sodium cacodylate buffer for 1 hr at RT and incubated overnight at 4°C. Next, they were rinsed 3 × 10 min with 0.1 M sodium cacodylate buffer, and post-fix in 2% OsO₄ in 0.1 M sodium cacodylate buffer for 1 hr at RT. Another rinse 3 × 10 min with 0.1 M sodium cacodylate buffer followed, and then worms were embedded in resin mold in histogel. Samples were dehydrated for 15 min each in 50%, 70%, 90%, 95%, and finally, two changes of 100% ethanol, cleared in two 15 min changes of propylene oxide and infiltrated in propylene oxide:epon (Embed812), as follows: (a) 3:1, 1 hr, (b) 1:1, 1 hr, (c) 1:3, 1 hr, (d) full strength, 2 hr or overnight, two changes. Finally, samples were embedded in beam capsules in full epon and polymerized at 60°C for 24 hr. Samples were imaged using a JEM-1400-plus transmission electron microscope (JEOL, Peabody, MA).

5.4. Worm Recording and Tracking

5.4.1. Recording. A 35 mm plate containing worms of a specific group was placed between the two electromagnets, as shown in Figure 6 so that the plate surface and, therefore, the worms were positioned close to the center of the electromagnets. First, a 200 s movie (1 frame/s) was recorded in the absence of MF (OFF state), and immediately after, a second 200 s movie (1 frame/s) was recorded with the MF on (ON state), using QCapture Pro software (QImaging, Surrey, Canada) and a Micropublisher3.3 RTV camera (QImaging, Surrey, Canada), mounted on an Olympus SZ61 microscope (Olympus, Tokyo, Japan). We recorded over 200 s intervals because we were interested in detecting the transient effect of MF on locomotion dynamics. The two

electromagnets used were a 4.0" Dia. Electromagnet, 12 VDC, and a 3.5" Dia. Electromagnet, 12 VDC, both from APW Company, Rockaway, NJ. Electromagnets were operated at 1.67 and 3 A, respectively, as indicated by the manufacturer, using a 1762 DC power supply (BK Precision, Yorba Linda, CA). By using a noncontact infrared thermometer (Omega Engineering, Norwalk, CT) we verified that the plate surface temperature remained constant throughout the recording period.

5.4.2. Tracking. Every movie was imported to MATLAB (MathWorks, Natick, MA) for postprocessing. Each worm was tracked individually. To this end, we developed a custom tracking code in MATLAB (Figure S3). In the first step, all frames were used to construct the movie background, which consisted of all the objects that did not move for long periods of time during the entire recording. Then, each frame was subtracted from the background to extract the foreground, which consisted of all moving objects. Next, the user was prompted with the initial frame of the movie, of which the background had already been subtracted, to select the worm to be tracked by the software. After the user selected the worm, the code created a small examining frame around it and excluded the targeted worm from the rest of the movie frame. Then, the cropped figure was converted to a binary image. After the binary image was enhanced, the shape of the binary object, i.e., the worm, and its global position were stored. Next, the code proceeded to the next movie frame and used the extracted global location of the worm as the center of the small examining frame. The small examining frame must be large enough to capture the motion of the worm in two successive movie frames. Since there was more than one worm freely moving in each experiment, there were occasions in which more than one object were included in the small examining frame. For such occasions, the user was prompted by the code to manually indicate again the worm to be tracked. This way, the worm that was initially selected to be tracked was always encapsulated by the examining frame. The code continued the tracking process until the last frame of the movie was processed, and it stored the shape of the worm and its global location for each frame. Once finished, the user runs the code again to track another worm.

The tracking code can be found at <https://github.com/mirzakhali/MultiWormTracker>.

5.5. Locomotion Analysis. The following features of *C. elegans* morphology and experimental setup properties were used for the quantification of *C. elegans* locomotion parameters.

5.5.1. Morphology Features

- (1) Length: the worm length was defined as the chain-code pixel length of worm skeleton, which was converted into mm.
- (2) Centroid: the worm density was assumed to be constant throughout its body, so the centroid of mass was the same as geometric centroid. Since the swing of the head or tail (first or last 1/12 chain-code length

part of the worm) can significantly influence centroid determination, they were ignored when computing the centroid.

5.5.2. Setup

- (1) Coordinates system: the x -axis was set along the direction of the MF, between the two electromagnets, and z -axis was normal to the plate, pointing upward (Figure 6). Thus, by applying the right-hand rule, the coordinates system was established. Since we did not identify head/tail orientation for the worms, the coordinates system was important for the detection of directionality.
- (2) Unit conversion: any feature regarding length was derived first in pixels. With a known length recorded with the same experimental setup, the conversion between pixels and microns was determined.

Locomotion-related parameters of interest were divided into three categories: posture features, motion features, and path features, as described extensively by Yemini et al. [59], with minor modifications. A brief description of the examined features follows below.

5.5.3. Posture Feature

- (1) Bend count: this metric ($bends_{num}$) corresponds to the number of bends along a single worm. First, the supplementary angles (Figure S4) were computed along the worm skeleton. Next, a Gaussian filter over each 1/12 of the chain-code length of the skeleton was applied to the supplementary angles to smooth out any high-frequency changes and was then normalized. The filter had a constant proportional to the reciprocal of the standard deviation, $\alpha = 2.5$. By checking the sequence of supplementary angles, the bend count was incremented whenever the angle reached 0° or changed sign. The check started from the first 1/12 segment to the last 1/12 segment to ignore small bends near the tail and the head.

5.5.4. Motion Features

- (1) Motion state: worm's motion state can be divided into two types, the forward/backward state and the paused state. The worm was considered to be in the forward/backward state when its instantaneous speed was greater or equal to 5% of its mean length per second, and it was considered in the paused state when the instantaneous speed was less than 5% of its mean length per second. Therefore, the ratio of the time the worm was in the forward/backward state over the total recording time, namely the fb_{ratio} , and the ratio of the time the worm was in the paused

state over the total recording time, namely the stay ratio $stay_{ratio}$, were calculated.

- (2) Speed: velocity is defined as the signed difference between a single worm's centroids of two sequential frames in the coordinate over the time gap between two frames (1 s) and can be projected on two orthogonal axes x and y in the plane of the plate (Figure 6). The absolute value of velocity and its components gave $speed$, $speed_x$, and $speed_y$, respectively.

5.5.5. Path Features

- (1) Path curvature: this metric is defined as the angle, in radians, of the worm's path divided by the distance traveled in microns. Three successive frames were used to approximate the start, middle, and end of the worm's instantaneous path curvature. The angle was measured by the difference in tangent angles between the second to last frame centroid and the first to the second frame centroid. Then, the path curvature was obtained by dividing the angle by the distance between the first and last centroid.
- (2) Range: range is defined as the distance between the worm's centroid and the centroid of the worm's path in each frame.

5.6. Statistical Analyses. Locomotion features were analyzed using parametric tests since the Anderson–Darling normality test p -value was larger than 0.05 for all samples, thus confirming the normality null hypothesis that the data are not inconsistent with a Gaussian distribution.

For each group or nematodes, each group being fed on a particular type of nanoparticles, as described earlier, tested worms were tracked in three independent experiments conducted on three experimental days (OFF1/ON1, OFF2/ON2, and OFF3/ON3). Therefore, for Group 100, animals fed on *E. coli* OP50 mixed with 100 nm-diameter iron core paramagnetic particles, $n = 33$ (individual experiments: $n_1 = 13$, $n_2 = 11$, $n_3 = 9$); for Group 1, animals fed on *E. coli* OP50 mixed with 1 μm -diameter paramagnetic particles, $n = 32$ (individual experiments: $n_1 = 14$, $n_2 = 10$, $n_3 = 8$); for Group 40, animals fed on *E. coli* OP50 mixed with 40 nm-diameter iron core paramagnetic particles, $n = 25$ (individual experiments: $n_1 = 10$, $n_2 = 7$, $n_3 = 8$); and for Group C, namely control animals, fed on plain food source *E. coli* OP50, $n = 30$ ($n_1 = 11$, $n_2 = 10$, $n_3 = 9$).

For each group, we compared results from the ON state and OFF state for each experiment separately, and for all three experiments combined (Figure 5). Comparisons were made by applying Student's t -test (unpaired for individual experiments, paired for combined data), and differences were considered statistically significant when $p \leq 0.05$. We considered a locomotion feature to be affected by internalized paramagnetic particles in the presence of MF only when there was a statistically significant difference detected

on at least two experiments *and* when comparing combined data.

To find out whether there are differences in locomotion features due to the presence of nanoparticles alone (in the absence of a MF), we compared the three groups of particle-fed nematodes to untreated worms, when the MF is OFF. Comparisons were made by one-way analysis of variance (ANOVA), graphs and ANOVA results are presented in Figures S4 and S5. No statistically significant difference was detected between untreated and particle-fed animals, in the absence of MF.

All analyses were performed in GraphPad Prism 9.0 (GraphPad Software, San Diego, CA, USA).

To design the experiment, we run a statistical power analysis, using G*Power opensource software (Figure S6). We prepared the sample size used in the experiments based on this estimation. We slightly increased the sample size number to ensure that we have enough worms, since some of them might be injured or lost during the process.

Data Availability

All data supporting the results are available upon reasonable request; code is available on GitHub as described in the manuscript.

Disclosure

The manuscript was already published as a poster [92] based on the link <https://www.biorxiv.org/content/10.1101/248369v2>. Ehsan Mirzakhali is presently at Bioengineering, University of Pennsylvania, Philadelphia, PA. Yang Zhang is presently at Robotics System Development, Carnegie Mellon University, Pittsburgh, PA.

Conflicts of Interest

The authors declare that they have no conflicts of interest.

Authors' Contributions

BE and EG conceived the idea; EG, EM, and BE designed the experiments; EG, EM, and YZ ran experiments; EM created tracking algorithm and ran simulations; YZ ran tracking algorithm, processed, and analyzed recordings; EG, YZ, and EM collected and analyzed data; EG and EM wrote the paper, with input from YZ. All authors reviewed and edited the manuscript and gave final approval for publication.

Acknowledgments

We thank Nikos Chronis, Kenn Oldham, and Jinhong Qu for the use of selected equipment and Syeda Maisa for helping with preliminary worm videos. Scanning electron microscopy was performed at the Electron Microbeam Analysis Laboratory (EMAL) with support from the University of Michigan College of Engineering; we thank John Mansfield, Kai Sun, and Haiping Sun for the training. Transmission

electron microscopy was performed at the Microscopy & Image Analysis Laboratory (MIL) at the University of Michigan Medical School; we are grateful to Jeff Harrison and Penelope Blakely for their help and guidance. We thank Surojit Sural for his input on power analysis and to Hannah Seidel and Elisa Frankel for feedback. We are particularly grateful to Hong Zhan for his help with TEM images interpretation. This work was supported by the Division of Civil, Mechanical and Manufacturing Innovation, National Sciences Foundation (award #1334908 to B.E.), and the University of Michigan Office of Research (grant #U055203 to E.G.). EG is the recipient of NIH-NIA award K01-AG057833. The content is solely the responsibility of the authors and does not necessarily represent the official views of the National Institutes of Health.

Supplementary Materials

Figure S1: Calibration of the parameters in COMSOL Multiphysics simulations to match the available data for magnet 1 (a) and magnet 2 (b) that are used in the experiments. Figure S2: All the components of the gradient of the magnetic field (MF) for the particles in the vertical (along the y -axis) and horizontal (along the x -axis) configuration. Figure S3: Locomotion analysis process. Figure S4: Comparison of particle-fed nematodes with untreated nematodes, for all locomotion features, in the absence of MF (OFF). Each graph presents combined data for all three experiments for each worm group for one locomotion feature. Figure S5: One-way ANOVA for the comparisons between all three groups of particle-fed animals against the untreated (control) group for the OFF state. OFF state for each of the three groups was compared against the control for each locomotion feature (see also Figure S4). Figure S6: Power analysis for locomotion dynamics experiments. (*Supplementary Materials*)

References

- [1] S. Ghodbane, A. Lahbib, M. Sakly, and H. Abdelmelek, "Bioeffects of static magnetic fields: oxidative stress, genotoxic effects, and cancer studies," *BioMed Research International*, vol. 2013, Article ID 602987, 12 pages, 2013.
- [2] F. T. Hong, "Magnetic field effects on biomolecules, cells, and living organisms," *Biosystems*, vol. 36, no. 3, pp. 187–229, 1995.
- [3] J. Shaw, A. Boyd, M. House et al., "Magnetic particle-mediated magnetoreception," *Journal of the Royal Society Interface*, vol. 12, no. 110, Article ID 20150499, 2015.
- [4] S. Ueno, P. Lövsund, and P. Å. Öberg, "Effects of alternating magnetic fields and low-frequency electric currents on human skin blood flow," *Medical and Biological Engineering and Computing*, vol. 24, pp. 57–61, 1986.
- [5] I. Öcal, T. Kalkan, and İ. Günay, "Effects of alternating magnetic field on the metabolism of the healthy and diabetic organisms," *Brazilian Archives of Biology and Technology*, vol. 51, no. 3, pp. 523–530, 2008.
- [6] N. A. Belova and D. Acosta-Avalos, "The effect of extremely low frequency alternating magnetic field on the behavior of

- animals in the presence of the geomagnetic field," *Journal of Biophysics*, vol. 2015, Article ID 423838, 8 pages, 2015.
- [7] J. Miyakoshi, "Effects of static magnetic fields at the cellular level," *Progress in Biophysics and Molecular Biology*, vol. 87, no. 2-3, pp. 213–223, 2005.
- [8] L. Teodori, J. Grabarek, P. Smolewski et al., "Exposure of cells to static magnetic field accelerates loss of integrity of plasma membrane during apoptosis," *Cytometry*, vol. 49, no. 3, pp. 113–118, 2002.
- [9] B. Lewczuk, G. Redlarski, A. Żak, N. Ziółkowska, B. Przybylska-Gornowicz, and M. Krawczuk, "Influence of electric, magnetic, and electromagnetic fields on the circadian system: current stage of knowledge," *BioMed Research International*, vol. 2014, Article ID 169459, 13 pages, 2014.
- [10] V. Zablotskii, T. Polyakova, O. Lunov, and A. Dejneka, "How a high-gradient magnetic field could affect cell life," *Scientific Reports*, vol. 6, Article ID 37407, 2016.
- [11] E. A. Osipova, V. V. Pavlova, V. A. Nepomnyashchikh, and V. V. Krylov, "Influence of magnetic field on zebrafish activity and orientation in a plus maze," *Behavioural Processes*, vol. 122, pp. 80–86, 2016.
- [12] D. Shcherbakov, M. Winkhofer, N. Petersen, J. Steidle, R. Hilbig, and M. Blum, "Magnetosensation in zebrafish," *Current Biology*, vol. 15, no. 5, pp. R161–R162, 2005.
- [13] E. Pascal Malkemper, S. H. K. Eder, S. Begall et al., "Magnetoreception in the wood mouse (*Apodemus sylvaticus*): influence of weak frequency-modulated radio frequency fields," *Scientific Reports*, vol. 5, Article ID 9917, 2015.
- [14] K. Kumari, M. Capstick, A. M. Cassara et al., "Effects of intermediate frequency magnetic fields on male fertility indicators in mice," *Environmental Research*, vol. 157, pp. 64–70, 2017.
- [15] G. Fedele, E. W. Green, E. Rosato, and C. P. Kyriacou, "An electromagnetic field disrupts negative geotaxis in *Drosophila* via a CRY-dependent pathway," *Nature Communications*, vol. 5, Article ID 4391, 2014.
- [16] M. Naito, S. Hirai, M. Mihara et al., "Effect of a magnetic field on *Drosophila* under supercooled conditions," *PLOS ONE*, vol. 1, no. 12, Article ID e51902, 2012.
- [17] E. Ramirez, J. L. Monteagudo, M. Garcia-Gracia, and J. M. R. Delgado, "Oviposition and development of *Drosophila* modified by magnetic fields," *Bioelectromagnetics*, vol. 4, no. 4, pp. 315–326, 1983.
- [18] P. G. Kale and J. W. Baum, "Genetic effects of strong magnetic fields in *Drosophila melanogaster*: II. Lack of interaction between homogeneous fields and fission neutron-plus-gamma radiation," *Environmental Mutagenesis*, vol. 2, no. 2, pp. 179–186, 1980.
- [19] J.-E. Bae, S. Bang, S. Min et al., "Positive geotactic behaviors induced by geomagnetic field in *Drosophila*," *Molecular Brain*, vol. 9, Article ID 55, 2016.
- [20] C. N. G. Giachello, N. S. Scrutton, A. R. Jones, and R. A. Baines, "Magnetic fields modulate blue-light-dependent regulation of neuronal firing by cryptochrome," *The Journal of Neuroscience*, vol. 36, no. 42, pp. 10742–10749, 2016.
- [21] B. H. H. Cheung, M. Cohen, C. Rogers, O. Albayram, and M. de Bono, "Experience-dependent modulation of *C. elegans* behavior by ambient oxygen," *Current Biology*, vol. 15, no. 10, pp. 905–917, 2005.
- [22] M. de Bono and C. I. Bargmann, "Natural variation in a neuropeptide Y receptor homolog modifies social behavior and food response in *C. elegans*," *Cell*, vol. 94, no. 5, pp. 679–689, 1998.
- [23] W. Liedtke, D. M. Tobin, C. I. Bargmann, and J. M. Friedman, "Mammalian TRPV4 (VR-OAC) directs behavioral responses to osmotic and mechanical stimuli in *Caenorhabditis elegans*," *PNAS*, vol. 100, no. Suppl. 2, pp. 14531–14536, 2003.
- [24] E. M. Hedgecock and R. L. Russell, "Normal and mutant thermotaxis in the nematode *Caenorhabditis elegans*," *PNAS*, vol. 72, no. 10, pp. 4061–4065, 1975.
- [25] A. Ward, J. Liu, Z. Feng, and X. Z. Shawn Xu, "Light-sensitive neurons and channels mediate phototaxis in *C. elegans*," *Nature Neuroscience*, vol. 11, pp. 916–922, 2008.
- [26] A. Vidal-Gadea, K. Ward, C. Beron et al., "Magnetosensitive neurons mediate geomagnetic orientation in *Caenorhabditis elegans*," *elife*, vol. 4, Article ID e07493, 2015.
- [27] Z. Njus, D. Feldmann, R. Brien, T. Kong, U. Kalwa, and S. Pandey, "Characterizing the effect of static magnetic fields on *C. elegans* using microfluidics," *Advances in Bioscience and Biotechnology*, vol. 6, no. 9, pp. 583–591, 2015.
- [28] X. Long, J. Ye, D. Zhao, and S.-J. Zhang, "Magnetogenetics: remote non-invasive magnetic activation of neuronal activity with a magnetoreceptor," *Science Bulletin*, vol. 60, no. 24, pp. 2107–2119, 2015.
- [29] L. Wang, H. Du, X. Guo et al., "Developmental abnormality induced by strong static magnetic field in *Caenorhabditis elegans*," *Bioelectromagnetics*, vol. 36, no. 3, pp. 178–189, 2015.
- [30] C.-H. Lee, Y.-C. Hung, and G. S. Huang, "Static magnetic field accelerates aging and development in nematode," *Communicative & Integrative Biology*, vol. 3, no. 6, pp. 528–529, 2010.
- [31] C. Bainbridge, B. L. Clites, C. S. Caldwell et al., "Factors that influence magnetic orientation in *Caenorhabditis elegans*," *Journal of Comparative Physiology A*, vol. 206, pp. 343–352, 2020.
- [32] C. Bainbridge, J. McDonald, A. Ahlert, Z. Benefield, W. Stein, and A. G. Vidal-Gadea, "Unbiased analysis of *C. elegans* behavior reveals the use of distinct turning strategies during magnetic orientation," *bioRxiv*, Article ID 688408, 2019.
- [33] M. Agotegaray, M. G. Blanco, A. Campelo et al., "β-cyclodextrin coating: improving biocompatibility of magnetic nanocomposites for biomedical applications," *Journal of Materials Science: Materials in Medicine*, vol. 31, Article ID 22, 2020.
- [34] J. Xu, K. Liu, T. Chen et al., "Rotating magnetic field delays human umbilical vein endothelial cell aging and prolongs the lifespan of *Caenorhabditis elegans*," *Aging*, vol. 11, no. 22, pp. 10385–10408, 2019.
- [35] C. G. Cranfield, A. Dawe, V. Karloukovski, R. E. Dunin-Borkowski, D. de Pomerai, and J. Dobson, "Biogenic magnetite in the nematode *Caenorhabditis elegans*," *Proceedings of the Royal Society B*, vol. 271, no. Suppl_6, pp. S436–S439, 2004.
- [36] P. Khare, M. Sonane, R. Pandey, S. Ali, K. C. Gupta, and A. Satish, "Adverse effects of TiO₂ and ZnO nanoparticles in soil nematode, *Caenorhabditis elegans*," *Journal of Biomedical Nanotechnology*, vol. 7, no. 1, pp. 116–117, 2011.
- [37] J. N. Meyer, C. A. Lord, X. Y. Yang et al., "Intracellular uptake and associated toxicity of silver nanoparticles in *Caenorhabditis elegans*," *Aquatic Toxicology*, vol. 100, no. 2, pp. 140–150, 2010.
- [38] J. H. Kim, S. H. Lee, Y. J. Cha et al., "*C. elegans*-on-a-chip for *in situ* and *in vivo* Ag nanoparticles' uptake and toxicity assay," *Scientific Reports*, vol. 7, Article ID 40225, 2017.
- [39] L. Gonzalez-Moragas, A. Roig, and A. Laromaine, "*C. elegans* as a tool for *in vivo* nanoparticle assessment," *Advances in Colloid and Interface Science*, vol. 219, pp. 10–26, 2015.

- [40] H. Ma, P. M. Bertsch, T. C. Glenn, N. J. Kabengi, and P. L. Williams, "Toxicity of manufactured zinc oxide nanoparticles in the nematode *Caenorhabditis elegans*," *Environmental Toxicology and Chemistry*, vol. 28, no. 6, pp. 1324–1330, 2009.
- [41] Y. Li, S. Yu, Q. Wu, M. Tang, Y. Pu, and D. Wang, "Chronic Al₂O₃-nanoparticle exposure causes neurotoxic effects on locomotion behaviors by inducing severe ROS production and disruption of ROS defense mechanisms in nematode *Caenorhabditis elegans*," *Journal of Hazardous Materials*, vol. 219–220, pp. 221–230, 2012.
- [42] Q. Wu, Y. Li, M. Tang, and D. Wang, "Evaluation of environmental safety concentrations of DMSA coated Fe₂O₃-NPs using different assay systems in nematode *Caenorhabditis elegans*," *PLOS ONE*, vol. 7, no. 8, Article ID e43729, 2012.
- [43] H. Huang, S. Delikanli, H. Zeng, D. M. Ferkey, and A. Pralle, "Remote control of ion channels and neurons through magnetic-field heating of nanoparticles," *Nature Nanotechnology*, vol. 5, pp. 602–606, 2010.
- [44] L. Wang, M. Wang, H. Du, Y. Liu, and A. Xu, "Lipid metabolism was interfered by phosphatidylcholine-coated magnetic nanoparticles in *C. elegans* exposed to 0.5 T static magnetic field," *Journal of Nanoscience and Nanotechnology*, vol. 17, no. 5, pp. 3172–3180, 2017.
- [45] E. Gourgou and N. Chronis, "Chemically induced oxidative stress affects ASH neuronal function and behavior in *C. elegans*," *Scientific Reports*, vol. 6, Article ID 38147, 2016.
- [46] G. Li, J. Gong, H. Lei, J. Liu, and X. Z. Shawn Xu, "Promotion of behavior and neuronal function by reactive oxygen species in *C. elegans*," *Nature Communications*, vol. 7, Article ID 13234, 2016.
- [47] J. Liu, B. Zhang, H. Lei et al., "Functional aging in the nervous system contributes to age-dependent motor activity decline in *C. elegans*," *Cell Metabolism*, vol. 18, no. 3, pp. 392–402, 2013.
- [48] A.-L. Hsu, Z. Feng, M.-Y. Hsieh, and X. Z. Shawn Xu, "Identification by machine vision of the rate of motor activity decline as a lifespan predictor in *C. elegans*," *Neurobiology of Aging*, vol. 30, no. 9, pp. 1498–1503, 2009.
- [49] L. Parida, S. Neogi, and V. Padmanabhan, "Effect of temperature pre-exposure on the locomotion and chemotaxis of *C. elegans*," *PLOS ONE*, vol. 9, no. 10, Article ID e111342, 2014.
- [50] J. T. Pierce-Shimomura, B. L. Chen, J. J. Mun, R. Ho, R. Sarkis, and S. L. McIntire, "Genetic analysis of crawling and swimming locomotory patterns in *C. elegans*," *PNAS*, vol. 105, no. 52, pp. 20982–20987, 2008.
- [51] A. Bansal, L. J. Zhu, K. Yen, and H. A. Tissenbaum, "Uncoupling lifespan and healthspan in *Caenorhabditis elegans* longevity mutants," *PNAS*, vol. 112, no. 3, pp. E277–E286, 2015.
- [52] B. B. Shtonda and L. Avery, "Dietary choice behavior in *Caenorhabditis elegans*," *Journal of Experimental Biology*, vol. 209, no. 1, pp. 89–102, 2006.
- [53] M. Peliti, J. S. Chuang, and S. Shaham, "Directional locomotion of *C. elegans* in the absence of external stimuli," *PLOS ONE*, vol. 8, no. 11, Article ID e78535, 2013.
- [54] J.-H. Hahm, S. Kim, R. DiLoreto et al., "*C. elegans* maximum velocity correlates with healthspan and is maintained in worms with an insulin receptor mutation," *Nature Communications*, vol. 6, Article ID 8919, 2015.
- [55] B. L. Clites and J. T. Pierce, "Identifying cellular and molecular mechanisms for magnetosensation," *Annual Review of Neuroscience*, vol. 40, pp. 231–250, 2017.
- [56] J. E. Park, S. Yoon, J. Jeon et al., "Multi-modal locomotion of *Caenorhabditis elegans* by magnetic reconfiguration of 3D microtopography," *Advanced Science*, vol. 9, no. 36, Article ID 2203396, 2022.
- [57] E. Mirzakhali, W. Nam, and B. I. Epureanu, "Reduced-order models for the dynamics of superparamagnetic nanoparticles interacting with cargoes transported by kinesins," *Nonlinear Dynamics*, vol. 90, pp. 425–442, 2017.
- [58] K. Nakata, Y. Hu, O. Uzun, O. Bakr, and F. Stellacci, "Chains of superparamagnetic nanoparticles," *Advanced Materials*, vol. 20, no. 22, pp. 4294–4299, 2008.
- [59] E. Yemini, T. Jucikas, L. J. Grundy, A. E. X. Brown, and W. R. Schafer, "A database of *Caenorhabditis elegans* behavioral phenotypes," *Nature Methods*, vol. 10, pp. 877–879, 2013.
- [60] Y. Li, L. Zhong, L. Zhang, X. Shen, L. Kong, and T. Wu, "Research advances on the adverse effects of nanomaterials in a model organism, *Caenorhabditis elegans*," *Environmental Toxicology and Chemistry*, vol. 40, no. 9, pp. 2406–2424, 2021.
- [61] L. Gonzalez-Moragas, S.-M. Yu, N. Benseny-Cases, S. Stürzenbaum, A. Roig, and A. Laromaine, "Toxicogenomics of iron oxide nanoparticles in the nematode *C. elegans*," *Nanotoxicology*, vol. 11, no. 5, pp. 647–657, 2017.
- [62] L. Gonzalez-Moragas, S.-M. Yu, E. Carenza, A. Laromaine, and A. Roig, "Protective effects of bovine serum albumin on superparamagnetic iron oxide nanoparticles evaluated in the nematode *Caenorhabditis elegans*," *ACS Biomaterials Science & Engineering*, vol. 1, no. 11, pp. 1129–1138, 2015.
- [63] D. Lim, J.-Y. Roh, H.-J. Eom, J.-Y. Choi, J. W. Hyun, and J. Choi, "Oxidative stress-related PMK-1 P38 MAPK activation as a mechanism for toxicity of silver nanoparticles to reproduction in the nematode *Caenorhabditis elegans*," *Environmental Toxicology and Chemistry*, vol. 31, no. 3, pp. 585–592, 2012.
- [64] W. Marimon-Bolívar, L. P. Tejada-Benítez, C. A. Núñez-Avilés, and D. D. De León-Pérez, "Evaluation of the in vivo toxicity of green magnetic nanoparticles using *Caenorhabditis elegans* as a biological model," *Environmental Nanotechnology, Monitoring & Management*, vol. 12, Article ID 100253, 2019.
- [65] S. Bosch, T. L. Botha, A. Jordaan, M. Maboeta, and V. Wepener, "Sublethal effects of ionic and nanogold on the nematode *Caenorhabditis elegans*," *Journal of Toxicology*, vol. 2018, Article ID 6218193, 11 pages, 2018.
- [66] A. Pluskota, E. Horzowski, O. Bossinger, and A. von Mikecz, "In *Caenorhabditis elegans* nanoparticle-bio-interactions become transparent: silica-nanoparticles induce reproductive senescence," *PLOS ONE*, vol. 4, no. 8, Article ID e6622, 2009.
- [67] Y.-F. Yang, Y.-J. Lin, and C.-M. Liao, "Toxicity-based toxicokinetic/toxicodynamic assessment of bioaccumulation and nanotoxicity of zerovalent iron nanoparticles in *Caenorhabditis elegans*," *International Journal of Nanomedicine*, vol. 12, pp. 4607–4621, 2017.
- [68] S. G. Donkin and P. L. Williams, "Influence of developmental stage, salts and food presence on various end points using *Caenorhabditis elegans* for aquatic toxicity testing," *Environmental Toxicology and Chemistry*, vol. 14, no. 12, pp. 2139–2147, 1995.
- [69] L. Landler, S. Nimpf, T. Hochstoeger, G. C. Nordmann, A. Papadaki-Anastasopoulou, and D. A. Keays, "Comment on "Magnetosensitive neurons mediate geomagnetic orientation in *Caenorhabditis elegans*,"" *eLife*, vol. 7, Article ID e30187, 2018.
- [70] A. Vidal-Gadea, C. Bainbridge, B. Clites et al., "Response to comment on "Magnetosensitive neurons mediate geomagnetic orientation in *Caenorhabditis elegans*,"" *eLife*, vol. 7, Article ID e31414, 2018.

- [71] A. G. Vidal-Gadea, C. S. Caldart, C. Bainbridge et al., “Temporal and spatial factors that influence magnetotaxis in *C. elegans*,” *bioRxiv*, pp. 1–23, 2018.
- [72] K. S. Kindt, K. B. Quast, A. C. Giles et al., “Dopamine mediates context-dependent modulation of sensory plasticity in *C. elegans*,” *Neuron*, vol. 55, no. 4, pp. 662–676, 2007.
- [73] E. R. Sawin, R. Ranganathan, and H. R. Horvitz, “*C. elegans* locomotory rate is modulated by the environment through a dopaminergic pathway and by experience through a serotonergic pathway,” *Neuron*, vol. 26, no. 3, pp. 619–631, 2000.
- [74] G. Voglis and N. Tavernarakis, “A synaptic DEG/ENaC ion channel mediates learning in *C. elegans* by facilitating dopamine signalling,” *The EMBO Journal*, vol. 27, no. 24, pp. 3288–3299, 2008.
- [75] A. Albeg, C. J. Smith, M. Chatzigeorgiou et al., “*C. elegans* multi-dendritic sensory neurons: morphology and function,” *Molecular and Cellular Neuroscience*, vol. 46, no. 1, pp. 308–317, 2011.
- [76] J. D. McGhee, “The *C. elegans* intestine,” in *WormBook: the online review of C. elegans biology*, The *C. elegans* Research Community, 2007.
- [77] S. Nagy, Y.-C. Huang, M. J. Alkema, and D. Biron, “*Caenorhabditis elegans* exhibit a coupling between the defecation motor program and directed locomotion,” *Scientific Reports*, vol. 5, Article ID 17174, 2015.
- [78] I. Mori, “Genetics of chemotaxis and thermotaxis in the nematode *Caenorhabditis elegans*,” *Annual Review of Genetics*, vol. 33, pp. 399–422, 1999.
- [79] A. J. Bretscher, K. E. Busch, and M. de Bono, “A carbon dioxide avoidance behavior is integrated with responses to ambient oxygen and food in *Caenorhabditis elegans*,” *PNAS*, vol. 105, no. 23, pp. 8044–8049, 2008.
- [80] J. Russell, A. G. Vidal-Gadea, A. Makay, C. Lanam, and J. T. Pierce-Shimomura, “Humidity sensation requires both mechanosensory and thermosensory pathways in *Caenorhabditis elegans*,” *PNAS*, vol. 111, no. 22, pp. 8269–8274, 2014.
- [81] A. Kuhara, N. Ohnishi, T. Shimowada, and I. Mori, “Neural coding in a single sensory neuron controlling opposite seeking behaviours in *Caenorhabditis elegans*,” *Nature Communications*, vol. 2, Article ID 355, 2011.
- [82] D. Liu, M. R. Maxey, and G. E. Karniadakis, “Simulations of dynamic self-assembly of paramagnetic microspheres in confined microgeometries,” *Journal of Micromechanics and Microengineering*, vol. 15, no. 12, Article ID 2298, 2005.
- [83] J. Liu, E. M. Lawrence, A. Wu et al., “Field-induced structures in ferrofluid emulsions,” *Physical Review Letters*, vol. 74, no. 14, pp. 2828–2831, 1995.
- [84] P. S. Doyle, J. Bibette, A. Bancaud, and J.-L. Viovy, “Self-assembled magnetic matrices for DNA separation chips,” *Science*, vol. 295, no. 5563, Article ID 2237, 2002.
- [85] V. Zablotskii, T. Syrovets, Z. W. Schmidt, A. Dejneka, and T. Simmet, “Modulation of monocytic leukemia cell function and survival by high gradient magnetic fields and mathematical modeling studies,” *Biomaterials*, vol. 35, no. 10, pp. 3164–3171, 2014.
- [86] S. Hughes, S. McBain, J. Dobson, and A. J. El Haj, “Selective activation of mechanosensitive ion channels using magnetic particles,” *Journal of the Royal Society Interface*, vol. 5, no. 25, pp. 855–863, 2008.
- [87] S. Shaham, “Methods in cell biology,” in *WormBook: the online review of C. elegans biology*, The *C. elegans* Research Community, 2006.
- [88] J. E. Sulston and J. Hodgkin, “Methods,” in *The Nematode Caenorhabditis elegans*, W. B. Wood, Ed., pp. 587–606, Cold Spring Harbor Laboratory Press, Cold Spring Harbor, NY, 1988.
- [89] D. H. Hall, V. P. Winfrey, G. Blaeuer et al., “Ultrastructural features of the adult hermaphrodite gonad of *Caenorhabditis elegans*: relations between the germ line and soma,” *Developmental Biology*, vol. 212, no. 1, pp. 101–123, 1999.
- [90] D. H. Hall, E. Hartwig, and K. C. Q. Nguyen, “Modern electron microscopy methods for *C. elegans*,” in *Methods in Cell Biology*, vol. 107, pp. 93–149, Academic Press, 2012.
- [91] A. L. Kovács, “The application of traditional transmission electron microscopy for autophagy research in *Caenorhabditis elegans*,” *Biophysics Reports*, vol. 1, pp. 99–105, 2015.
- [92] E. Gourgou, Y. Zhang, E. Mirzakhilili, and B. Epureanu, “*Caenorhabditis elegans* locomotion is affected by internalized paramagnetic nanoparticles in the presence of magnetic field,” *bioRxiv*, Article ID 248369, 2019.